Strong coupling between inviscid fluid and boundary layer for airfoils with sharp leading edge. I - 2D Incompressible steady case

J.-J. Angelini, Christian Soize

STRONG COUPLING BETWEEN INVISCID FLUID AND BOUNDARY LAYER FOR AIRFOILS WITH SHARP LEADING EDGE. I: 2-D INCOMPRESSIBLE STEADY CASE

by

J.J. ANGELINI (*) and C. SOIZE (*)

ABSTRACT

We consider here the strong coupling between inviscid fluid and two-dimensional boundary layer in cascade aeroelasticity problems. As a significant situation, we take the upper surface boundary layer separated at the leading edge and reattached before the trailing edge. In this first part, we study the incompressible steady case. The aim is to develop the mathematical and physical model using experiments made on a flat plate with sharp leading edge with four degrees of incidence at a Reynolds number of 400,000. The assumptions and the construction of the physical and mathematical model are given along with the numerical analysis, and we compare the experiments with numerical results.

Keywords (NASA thesaurus): Aerodynamics — Aerolasticity — Boundary layer flow.

(*) ONERA, BP n° 72, 92322 Châtillon Cedex.

I. —INTRODUCTION

In the framework of cascade aeroelasticity problems [40, 41], the comparisons of experimental results with the predictions given by numerical models are not satisfactory if the model takes into account only the inviscid fluid but not the upper surface boundary layer. In effect, in the case of an airfoil with a sharp leading edge at a positive angle of attack, not completely stalled (situation investigated here), the upper surface boundary layer separates on the leading edge and reattaches on the airfoil. Analysis of the experimental results shows that it is the separated-reattached situation which modifies the phases and that modeling with an inviscid fluid alone is therefore not sufficient to predict the aeroelastic instabilities. In this case, it is necessary to include the upper surface boundary layer in the model and to take the inviscid fluid/boundary layer strong coupling into account in the unsteady model with separation on the leading edge and reattachment on the airfoil, using a two-dimensional model.

Mathematical and physical models as well as operational programs exist for strong coupling in the 2D incompressible and compressible case. For instance, defective integral equation (EDI) methods were developed at ONERA [25-32] and much research has been done on the mathematical and physical models of the boundary layer [2, 3, 15].

In the separated-reattached situation, there is a large amount of turbulence in the boundary layer, in particular in the upstream separated region. It has a significant effect on determination of the position of the reattachment point on the airfoil, and it seems to be the fluctuations of this position which cause phase modifications in the unsteady case. It is therefore necessary to correctly account for this phenomenon in the model, which leads to modifying the transport equations and modeling a turbulence term which appears in the Karman equation. In addition, conventional models seem to have difficulty in representing the physics in the initial percentages of the upper surface near the leading edge. For this reason, we chose an appropriate model based on experimental results. Finally, this situation requires modifying the solving methods for strong coupling, as the separated-reattached situation is very different from the attached-separated situation from the standpoint of the mathematical nature of the equations, which affects the solving schemes.

As was indicated, the case considered requires revising certain points of the physical model, the mathematical model and the solving methods.

This part I concerns study of the 2D incompressible steady case. It is aimed at developing the model which will be used as basis for the developments relative to the aeroelasticity problems and therefore for the compressible or incompressible unsteady model.

All these developments were established and verified mainly based on the measurements made in the steady case [3] on a flat plate with leading and trailing edges beveled on one side for a 4-degree angle of attack and a Reynolds number of approximately 400,000, as we had pressure coefficients as well as upper surface boundary layer parameters (displacement and momentum thicknesses, form parameter, integral turbulent friction, turbulence integral). We also used another experimental base, i. e. the measurements made in the steady case [43] on the Pflenminger-Sulzer (PFSU) blade profile, with an angle of attack varying from 4 to 7 degrees for a Reynolds number of approximately 2,500,000. For these measurements we actually had only Cps and we used these results only qualitatively, mainly to check the region of the reattachment point according to the angle of attack and the angle above which stalling occurred. However, we give experimental comparisons for the Cps of PFSU.

II. —MODEL CONSTRUCTION DATA AND HYPOTHESES

We consider an airfoil with a sharp leading edge, a chord L, an angle of attack α_1, in a flow at a velocity $\hat{\mathbb{V}}_\infty$, with a Reynolds number $\mathscr{R} = \rho \| \hat{\mathbb{V}}_\infty \| L/\mu$. All the parameters of the problem are made dimensionless. The geometry of the dimensionless airfoil with unit chord is identified in a reference system OXZ, where O is the leading edge and OX is the chord. We therefore have $\mathbb{V}_\infty = (\cos \alpha_I, \sin \alpha_I)$ and $\| \mathbb{V}_\infty \| = 1$. A curvilinear abcissa x with origin O is defined on the airfoil, positioned to cover the upper surface from O to the trailing edge F and the lower surface from F to O. The curvilinear abscissa of F corresponding to $X = 1$ is noted x_F. The upper surface is described for $x \in]O, x_F[$ and the lower surface for $x \in]x_F, x_T[$. We consider the local orthonormal curvilinear reference system $(\mathbf{xx'}, \mathbf{xz})$ whose origin is the curvilinear abscissa x, with $\mathbf{xx'}$ tangent to the wall and $\mathbf{xz}$ pointing along the external normal.

The hypotheses of the model corresponding to [3] are as follows:

(H1) The airfoil has a sharp leading edge at a positive angle of attack.

(H2) The flow is steady, incompressible, 2D at a high Reynolds number.

(H3) The upper surface boundary layer is a turbulent thin 2D layer separated at the leading edge and reattached on the airfoil.

The upper surface curvature terms can be neglected in the boundary layer equations.

(H4) The lower surface boundary layer may not be taken into account in the model.

(H5) The external inviscid fluid flow is potential.

III. —MODEL FOR THE UPPER SURFACE BOUNDARY LAYER

III,1. — BASIC EQUATIONS OF THE MODEL

The equations of the model are the averaged Navier-Stokes equations with incompressible constant viscosity (NSMI) for a turbulent thin 2D boundary layer in the vicinity of a flat wall and at a high Reynolds number. Generally, the terms related to the turbulent kinetic energy are neglected in these equations, but for the reasons already stated, we keep these terms in the NSMI. They have the effect of coupling the Karman equation with the transport equations. To the NSMI equations must be added three transport equations whose closure is conventionally provided by modeling. Considering (H3), the upper surface boundary layer is a flat wall. We therefore establish the equations for a flat wall and use them directly in the local curvilinear reference system of the airfoil upper surface. Space $\mathbb{R}^3$ is therefore referenced to a cartesian reference system $Oxyz$; the flat wall is in plane Oxy, the main direction of the flow is Ox, the boundary layer is on side $z>0$, and the 2D flow plane is plane Oxz. u, v, w are the velocity components in $Oxyz$, p is the pressure and ρ is the density. If A designates one of the values, we write $A=\bar{A}+A'$ where $\bar{A}=\langle A\rangle$ is the mean value and A' is the fluctuation. In the incompressible case, $\rho'=0$ and $\rho=\bar{\rho}$. As the viscosity is constant, $\mu'=0$, the dynamic viscosity coefficient $\mu=\bar{\mu}$ and $\bar{\nu}=\mu/\rho$. In the framework of the above hypotheses, the NSMI equations are written:

$$\frac{\partial \bar{u}}{\partial x}+\frac{\partial \bar{w}}{\partial z}=0 \tag{1}$$

$$\rho\frac{\partial \bar{u}}{\partial t}+\rho\frac{\partial}{\partial x}(\bar{u}^2)+\rho\frac{\partial}{\partial z}(\bar{u}\bar{w}) =-\frac{\partial \bar{p}}{\partial x}+\frac{\partial \bar{\tau}}{\partial z}-\frac{\partial}{\partial x}(\rho\langle u'^2\rangle) \tag{2}$$

$$\rho\frac{\partial \bar{w}}{\partial t}+\rho\frac{\partial}{\partial x}(\bar{u}\bar{w})+\rho\frac{\partial}{\partial z}(\bar{w}^2) =-\frac{\partial \bar{p}}{\partial z}-\frac{\partial}{\partial z}(\rho\langle w'^2\rangle) \tag{3}$$

where:

$$\bar{\tau}_{lam}=\mu\frac{\partial \bar{u}}{\partial z};\qquad \tau_{tur}=-\rho\langle u'w'\rangle \tag{4}$$

$$\bar{\tau}=\bar{\tau}_{lam}+\tau_{tur} \tag{5}$$

where $\bar{\tau}_{lam}$ is the laminar viscous friction, τ_{tur} is the turbulent friction and $\bar{\tau}$ is the total friction. K and $\mathscr{E}$ are the kinetic energy and the turbulent dissipation term per mass unit respectively:

$$K=\frac{1}{2}(\langle u'^2\rangle+\langle v'^2\rangle+\langle w'^2\rangle) \tag{6}$$

$$\mathscr{E}=\nu\left(\left\langle\left(\frac{\partial u'}{\partial x}\right)^2\right\rangle+\left\langle\left(\frac{\partial v'}{\partial y}\right)^2\right\rangle+\left\langle\left(\frac{\partial w'}{\partial z}\right)^2\right\rangle\right). \tag{7}$$

For closure of the three 2D transport equations in K, τ_{tur} and $\mathscr{E}$, we use the model proposed in [9, 23, 24, 46] for the incompressible turbulent thin 2D layers. These equations are written:

$$\left.\begin{aligned}
&\frac{\partial}{\partial t}\left(\frac{\tau_{tur}}{\rho}\right)+\bar{u}\frac{\partial}{\partial x}\left(\frac{\tau_{tur}}{\rho}\right)+\bar{w}\frac{\partial}{\partial z}\left(\frac{\tau_{tur}}{\rho}\right)\\
&\qquad=C_{\tau_1}K\frac{\partial \bar{u}}{\partial z}-C_{\tau_2}\frac{\mathscr{E}}{K}\left(\frac{\tau_{tur}}{\rho}\right)+\frac{\partial}{\partial z}J_{\tau_{tur}}\\
&\frac{\partial K}{\partial t}+\bar{u}\frac{\partial K}{\partial x}+\bar{w}\frac{\partial K}{\partial z}=\left(\frac{\tau_{tur}}{\rho}\right)\frac{\partial \bar{u}}{\partial z}-\mathscr{E}+\frac{\partial}{\partial z}J_K\\
&\frac{\partial \mathscr{E}}{\partial t}+\bar{u}\frac{\partial \mathscr{E}}{\partial x}+\bar{w}\frac{\partial \mathscr{E}}{\partial z}=C_{\varepsilon_1}\frac{\mathscr{E}}{K}\left(\frac{\tau_{tur}}{\rho}\right)\frac{\partial \bar{u}}{\partial z}\\
&\qquad-C_{\varepsilon_2}\frac{\mathscr{E}^2}{K}+\frac{\partial}{\partial z}J_\varepsilon
\end{aligned}\right\} \tag{8}$$

$$\left.\begin{aligned}
&J_{\tau_{tur}}=\frac{\nu_t}{\sigma_{\tau_{tur}}}\frac{\partial}{\partial z}\left(\frac{\tau_{tur}}{\rho}\right);\qquad J_K=\frac{\nu_t}{\sigma_K}\frac{\partial K}{\partial z};\\
&J_\varepsilon=\frac{\nu_t}{\sigma_\varepsilon}\frac{\partial \mathscr{E}}{\partial z};\qquad \sigma_{\tau_{tur}}=0{,}9;\\
&\sigma_K=1;\qquad \sigma_\varepsilon=1.3
\end{aligned}\right\} \tag{9}$$

$$\left.\begin{aligned}
&C_{\tau_1}=(2a_1)^2C_{\tau_2};\qquad a_1=0{,}15;\\
&C_{\tau_2}=1{,}5;\qquad C_{\varepsilon_1}=1{,}275;\qquad C_{\varepsilon_2}=1{,}8
\end{aligned}\right\} \tag{10}$$

$$\nu_t=(2a_1K)^{1/2}l;\qquad \mathscr{E}=\frac{(2a_1)^{3/2}}{l}K^{3/2}. \tag{11}$$

By eliminating length l between the two equations (11), substituting the expression of ν_t thus obtained in (9) and taking equation (1) into account, equations (8) are written:

$$\begin{aligned}
&\frac{\partial}{\partial t}\left(\frac{\tau_{tur}}{\rho}\right)+\frac{\partial}{\partial x}\left(\bar{u}\frac{\tau_{tur}}{\rho}\right)+\frac{\partial}{\partial z}\left(\bar{w}\frac{\tau_{tur}}{\rho}\right)\\
&\qquad=-1{,}5\frac{\mathscr{E}}{K}\left(\frac{\tau_{tur}}{\rho}-0{,}09\frac{K^2}{\mathscr{E}}\frac{\partial \bar{u}}{\partial z}\right)\\
&\qquad+\frac{\partial}{\partial z}\left(0{,}1\frac{K^2}{\mathscr{E}}\frac{\partial}{\partial z}\left(\frac{\tau_{tur}}{\rho}\right)\right)
\end{aligned} \tag{12}$$

$$\frac{\partial K}{\partial t}+\frac{\partial}{\partial x}(\bar{u}K)+\frac{\partial}{\partial z}(\bar{w}K)$$
$$=\left(\frac{\tau_{tur}}{\rho}\right)\frac{\partial \bar{u}}{\partial z}-\mathscr{E}+\frac{\partial}{\partial z}\left(0{,}09\frac{K^2}{\mathscr{E}}\frac{\partial K}{\partial z}\right) \quad (13)$$

$$\frac{\partial \mathscr{E}}{\partial t}+\frac{\partial}{\partial x}(\bar{u}\mathscr{E})+\frac{\partial}{\partial z}(\bar{w}\mathscr{E})$$
$$=-1{,}5\frac{\mathscr{E}}{K}\left(1{,}2\mathscr{E}-0{,}85\left(\frac{\tau_{tur}}{\rho}\right)\frac{\partial \bar{u}}{\partial z}\right)$$
$$+\frac{\partial}{\partial z}\left(\frac{0{,}09}{1{,}3}\frac{K^2}{\mathscr{E}}\frac{\partial \mathscr{E}}{\partial z}\right). \quad (14)$$

III,2. — STEADY INCOMPRESSIBLE 2D DEFECTIVE INTEGRAL EQUATIONS

The defective formulation and the approximated defective integral method developed in [27, 28, 29, 30] are used with the assumptions of an incompressible steady turbulent thin 2D layer for a flat wall. With the viscous variables $\bar{u}$, $\bar{w}$, $\bar{p}$, ρ are associated inviscid fluid variables u, w, p, ρ defined in the same space domain (here $\rho=\bar{\rho}$)) and verifying the steady incompressible 2D Euler equations (EUI). In addition, the asymptotic conditions at infinity in direction Oz normal to the wall were imposed on these variables.

$$\left.\begin{array}{c}\lim_{z\to+\infty}(\varphi(x,z)-\bar{\varphi}(x,z))=0,\\ \varphi\in\{u,w,p\}.\end{array}\right\} \quad (15)$$

Subtracting (NSMI) from (EUI) and using the thin layer approximation gives a first-order approximation of the defective equations:

$$\frac{\partial}{\partial x}(\rho u-\rho\bar{u})+\frac{\partial}{\partial z}(\rho w-\rho\bar{w})=0 \quad (16)$$

$$\frac{\partial}{\partial x}(\rho u^2-\rho\bar{u}^2)+\frac{\partial}{\partial z}(\rho uw-\rho\bar{u}\bar{w})$$
$$+\frac{\partial}{\partial x}(p-\bar{p})=-\frac{\partial\bar{\tau}}{\partial z}+\frac{\partial}{\partial x}(\rho\langle u'^2\rangle) \quad (17)$$

$$\frac{\partial}{\partial z}(p-\bar{p})=\frac{\partial}{\partial z}(\rho\langle w'^2\rangle). \quad (18)$$

Integrating equations (18), (16) and (17) in z from 0 to $+\infty$, and using (15) gives (1) a relation between the inviscid and viscous pressure fields, (2) the strong coupling relation (RLCF) between the inviscid velocity field, the viscous velocity field and the displacement thickness $\delta_1(x)$, (3) the Karman equation (EQK). Developing the local defective equation (17) on the line with equation $z=\delta(x)$, where $\delta_1(x)$ is the thickness of the boundary layer, using (16) and writing the equivalent of (15) on this line for u and w gives the entrainment equation (EQE). However, we also use an approximated form of EQE called (EQEA), obtained by integrating (1) in z from 0 to $\delta(x)$ and using EQE.

The inviscid fluid velocity modulus is noted $q(x, z)$ and, for $z=0$, this modulus is noted $Q(x)$:

$$\left.\begin{array}{c}q(x,z)=(u(x,z)^2+w(x,z)^2)^{1/2}\\ Q(x)=q(x,0).\end{array}\right\} \quad (19)$$

The displacement thickness $\delta_1(x)$ and momentum thickness $\theta(x)$ are such that:

$$\rho Q(x)\delta_1(x)=\int_0^{+\infty}(\rho u-\rho\bar{u})_{(x,z)}dz \quad (20)$$

$$\left.\begin{array}{c}\rho Q(x)^2(\delta_1(x)+\theta(x))\\ =\int_0^{+\infty}(\rho u^2-\rho\bar{u}^2)_{(x,z)}dz.\end{array}\right\} \quad (21)$$

The form parameter of the layer is conventionally noted $H(x)$ and $\alpha(x)$ such that:

$$H(x)=\frac{\delta_1(x)}{\theta(x)};\qquad \alpha(x)=\frac{\delta_1(x)}{\delta(x)}. \quad (22)$$

The friction $C_F(x)$, entrainment $C_E(x)$ and global dissipation $\Phi(x)$ coefficients are defined by:

$$\frac{C_F(x)}{2}=\frac{\bar{\tau}(x,0)}{\rho Q(x)^2} \quad (23)$$

$$C_E(x)=\frac{(\partial\bar{\tau}/\partial z)_{(x,\delta(x))}}{\rho q(x,\delta(x))(\partial/\partial z(u-\bar{u}))_{(x,\delta(x))}} \quad (24)$$

$$\Phi(x)=\frac{2}{\rho Q(x)^3}\int_0^{+\infty}\left(\bar{\tau}\frac{\partial\bar{u}}{\partial z}\right)_{(x,z)}dz. \quad (25)$$

Finally, $\mathscr{T}(x)$ denotes the integral related to turbulence such that:

$$\mathscr{T}(x)=\int_0^{+\infty}(\rho\langle u'^2\rangle-\rho\langle w'^2\rangle)_{(x,z)}dz. \quad (26)$$

Neglecting the external turbulence and developing the wall boundary condition $\bar{w}(x,0)=0$ for $x\in[0, x_F]$, the equations relating the pressures, RCLF, EQK, EQE and EQEA, are written:

$$\begin{array}{l}p(x,z)=\bar{p}(x,z)+\rho\langle w'^2\rangle(x,z)\\ p(x,z)=\bar{p}(x,z)+\rho\langle w'^2\rangle(x,z)\end{array} \quad (27)$$

$$\frac{d}{dx}\{Q(x)\delta_1(x)\}=w(x,0) \quad (28)$$

$$\frac{d}{dx}\{\rho Q(x)^2(\delta_1(x)+\theta(x))\}-\rho(uw)_{(x,\,0)}$$

$$=\rho Q(x)^2\frac{C_F(x)}{2}+\frac{d}{dx}\mathscr{T}(x) \quad (29)$$

$$(\rho u)_{(x,\,\delta(x))}\frac{d\delta(x)}{dx}-(\rho w)_{(x,\,\delta(x))}$$

$$=(\rho q)_{(x,\,\delta(x))}\times C_E(x) \quad (30)$$

$$\frac{d}{dx}\{\rho Q(x)(\delta(x)-\delta_1(x))=\rho Q(x)C_E(x). \quad (31)$$

As was mentioned, EQK contains an integral term $\mathscr{T}(x)$ related to the turbulent kinetic energy.

III,3. — ALGEBRAIC CLOSURE

The use of EQK and EQE requires the introduction of an algebraic closure since there are more unknowns in the problem than there are equations.

III,3,1. — Profile of the mean velocity and friction coefficient

We use the model proposed in [28] for attached or separated, incompressible or compressible turbulent 2D boundary layers. This model covers the complete domain $1<H<+\infty$ and models the profiles with reverse flow. In the incompressible case, this model leads to the following formulation in which all the values depend on x, but we have omitted x to simplify the expression. We note as η the dimensionless ordinate, as $\mathscr{R}_{\delta_1}$ and $\mathscr{R}_\delta$ the Reynolds numbers associated with δ_1 and δ:

$$\eta=\frac{z}{\delta}, \qquad \mathscr{R}_{\delta_1}=\mathscr{R}Q\delta_1, \qquad \mathscr{R}_\delta=\frac{1}{\alpha}\mathscr{R}_{\delta_1}. \quad (32)$$

Denoting as $\mathrm{Sg}(x)$ the "sign of x" function, the mean velocity profile and C_F are written:

$$\frac{\bar{q}(\eta)}{Q}=1-C_2\tilde{F}(\eta)+C_1\,\mathrm{Log}\,\eta \quad (33)$$

$$C_F=2(0{,}41\,C_1)^2(\mathrm{Sg}\,C_1). \quad (34)$$

where:

$$\tilde{F}(\eta)=\begin{cases} F\left(\dfrac{\eta-\eta^*}{1-\eta^*}\right) & \text{if} \quad \eta^*<\eta\leqq 1 \\ 1 \quad \text{if} \quad 0\leqq\eta\leqq\eta^* \\ F(\eta)=(1-\eta^{3/2})^2. \end{cases}$$

Function $\alpha\mapsto\eta^*(\alpha)$ is such that:

$$\left.\begin{array}{l} \eta^*=0 \quad \text{if} \quad 0<\alpha\leqq 0{,}44 \\ \text{(boundary layer attached in } x\text{)} \\ \eta^*=4{,}598\,(\alpha-0{,}44) \quad \text{if} \quad 0{,}44<\alpha\leqq 0{,}69 \\ \eta^*=2{,}299\,(\alpha-0{,}565) \quad \text{if} \quad 0{,}69<\alpha<1 \\ \text{(boundary layer separated in } x\text{)}. \end{array}\right\} \quad (36)$$

Constant $C_1(x)$ is obtained by solving the equation:

$$C_1=\frac{1-C_3\alpha}{\mathrm{Log}(0{,}41\,\mathscr{R}_{\delta_1}|C_1|/\alpha)+5{,}25\times 0{,}41-C_3} \quad (37)$$

where:

$$C_3=\frac{2{,}22}{1+1{,}22\,\eta^*} \quad (38)$$

and constant C_2 is given by:

$$C_2=1-C_1\left\{5{,}25\times 0{,}41+\mathrm{Log}\left(0{,}41\,\mathscr{R}_{\delta_1}\frac{|C_1|}{\alpha}\right)\right\}. \quad (39)$$

We will use these closure equations described below. $\mathscr{R}_{\delta_1}$ and α are fixed in a point x.

We compute η^* by (36), C_3 by (38), C_1 by solving (37), C_2 by (39). We determine $\bar{q}$ and C_F by (33) and (34).

III,3,2. — Expression of the form parameter H

Using the thin layer approximation, we have, starting from (21) in x fixed:

$$Q^2(\delta_1+\theta)\simeq Q^2\int_0^\delta\left(\frac{u^2}{Q^2}-\frac{\bar{u}^2}{Q^2}\right)dz$$

$$\simeq Q^2\int_0^\delta\left(1-\frac{\bar{q}(z)^2}{Q^2}\right)dz.$$

Considering the definition (22) of H, this gives:

$$\alpha\left(1+\frac{1}{H}\right)\simeq\int_0^1\left(1-\left(\frac{\bar{q}(\eta)}{Q}\right)^2\right)d\eta.$$

Substituting the expression of the mean profile (33) gives, after making all the calculations:

$$\alpha\left(\frac{1}{H}-1\right)=-C_2^2[\eta^*+2A_6(1-\eta^*)]-2C_1^2$$

$$+2C_1C_2[\eta^*(\mathrm{Log}\,\eta^*-1)+2(1-\eta^*)A(\eta^*)] \quad (40)$$

where:

$$A(\eta^*) = -\frac{1}{2}\left[A_1 B_* + A_2 + A_3 \lambda_* + A_4 \lambda_*^2 + A_1 \lambda_* B_* \text{ Log } \eta^* + A_5 \lambda_*^{5/2} \text{ Arctan } \frac{1}{\sqrt{\lambda_*}} \right]$$

$$\lambda_* = \eta^* (1-\eta^*)^{-1}; \qquad B_* = 4 - \lambda_*^3;$$

$$A_1 = 0.25; \qquad A_2 = -0.2575; \qquad A_3 = 0.45;$$

$$A_4 = -1.475; \qquad A_5 = 1.6; \qquad A_6 = 0.1578.$$

III,3,3. — *Modeling of the entrainment coefficient and total dissipation for an equilibrium turbulent boundary layer at a high Reynolds number*

For an equilibrium turbulent boundary layer, coefficient $C_E(x)$ defined by (24) is noted $C_{E_{eq}}(x)$ and the dissipation $\Phi(x)$ defined by (25) is noted $\Phi_{eq}(x)$. For high Reynolds numbers, we use the model proposed in [28] which is adapted to separation. This model is constructed with the profile equation (33) and a mixing length model for $\bar{\tau}$ based on the scale $\tilde{\delta}$ such that:

$$\tilde{\delta}(x) = (1-\eta^*(x))\,\delta(x) = (1-\eta^*(x))\frac{\delta_1(x)}{\alpha(x)}. \quad (41)$$

For a flat wall boundary layer in the incompressible case without correction factor for external turbulence effects, this model is written:

$$C_{E_{eq}} = 0{,}053\, C_3\, \alpha - 0{,}182 \times 0{,}41 \times \sqrt{2} \times C_1 \quad (42)$$

$$\Phi_{eq} = |u_p|\,|C_F| + 0{,}018\,(1-u_p^3)^3 \quad (43)$$

where:

$$u_p = 1 - C_3\,\alpha. \quad (44)$$

III,3,4. — *Modeling for a turbulent boundary layer out of equilibrium*

To use EQK and EQEA, it is necessary to introduce a model of $\mathcal{T}(x)$ and $C_E(x)$ which differ from the equilibrium values for boundary layers which are not in equilibrium. We again use hypotheses (H2) and (H3).

A. Model construction assumptions

In the turbulent part of the boundary layer, we have $\bar{\tau} \sim \tau_{tur} = -\rho \langle u' w' \rangle$ and we can neglect the corrections which would have to be made for the region located in the vicinity of the wall. Taking $f(x, z)$ such that:

$$f(x, z) \in \left\{ \frac{1}{\rho}\tau_{tur}(x, z),\ K(x, z),\ \mathscr{E}(x, z) \right\} \quad (45)$$

for a turbulence not in equilibrium and $f_{eq}(x, z)$ as the corresponding value for an equilibrium turbulence:

$$f_{eq}(x, z) \in \left\{ \frac{1}{\rho}\tau_{tur,\ eq}(x, z),\ K_{eq}(x, z),\ \mathscr{E}_{eq}(x, z) \right\}. \quad (46)$$

we can always define $g(x, z)$ such that:

$$f(x, z) = f_{eq}(x, z)\, g(x, z). \quad (47)$$

We then use the one-dimensional approximation of $g(x, z)$ proposed in [28] which consists of writing for $z \in (0, \delta(x))$:

$$\frac{f(x, z)}{f_{eq}(x, z)} = g(x, z) \simeq \tilde{g}(x) = \frac{\tilde{f}(x)}{\tilde{f}_{eq}(x)} \quad (48)$$

the one-dimensional model $\tilde{f}_{eq}(x)$ of $f_{eq}(x, z)$ being defined by:

$$\int_0^{\delta(x)} f_{eq}(x, z)\, dz \simeq \int_{(\eta^*\delta)(x)}^{\delta(x)} f_{eq}(x, z)\, dz = \tilde{\delta}(x)\, \tilde{f}_{eq}(x) \quad (49)$$

with $\tilde{\delta}(x)$ defined by (41). Using (48) and (49) yields:

$$\int_0^{\delta(x)} f(x, z)\, dz \simeq \int_{(\eta^*\delta)(x)}^{\delta(x)} f(x, z)\, dz \simeq \tilde{f}(x)\, \tilde{\delta}(x) \quad (50)$$

where $\tilde{f}(x)$ is the 1D approximation of $f(x, z)$. We set:

$$\tilde{\tau}(x) = \frac{1}{\rho}\tilde{\tau}_{tur}(x); \qquad \tilde{\tau}_{eq}(x) = \frac{1}{\rho}\tilde{\tau}_{tur,\ eq}(x)$$

$$\tau(x) = \frac{\tilde{\tau}(x)}{\tilde{\tau}_{eq}(x)} = \frac{\tilde{\tau}_{tur}(x)}{\tilde{\tau}_{tur,\ eq}(x)}; \quad (51)$$

$$k(x) = \frac{\tilde{K}(x)}{\tilde{K}_{eq}(x)}; \qquad \varepsilon(x) = \frac{\tilde{\mathscr{E}}(x)}{\tilde{\mathscr{E}}_{eq}(x)}.$$

which gives the following model:

$$C_E(x) = \tau(x)\, C_{E_{eq}}(x) \quad (52)$$

$$\Phi(x) = \tau(x)\, \Phi_{eq}(x). \quad (53)$$

To close the model it is necessary: (1) to have a model of the equilibrium values $\tilde{\tau}_{eq}(x)$, $\tilde{K}_{eq}(x)$ and $\tilde{\mathscr{E}}_{eq}(x)$; (2) to determine equations for $\tau(x)$, $k(x)$ and $\varepsilon(x)$ from the local transport equations (12)-(14); (3) to construct a model of $\mathcal{T}(x)$ defined by (26).

B. ID Approximation of the Mean Profile and Its Gradient

Applying definition (50) of the 1D approximation to $\bar{u}$ and $\frac{\partial \bar{u}}{\partial z}$, writing $\bar{u}(\eta)/Q \sim \bar{q}(\eta)/Q$ and using (33)

gives, considering the fact that $\int_0^1 F(u)\,du = 9/20 \sim 1/2$.

$$\widetilde{(\bar{u}(x,z))}(x) = Q(x)\left[\frac{1{,}22+1-C_2}{2{,}22} - C_1 - \frac{C_1}{1-\eta^*}\eta^* \text{ Log } \eta^*\right]$$

$$\left(\widetilde{\frac{\partial \bar{u}(x,z)}{\partial z}}\right)(x) = Q(x)\left(\frac{C_2 - C_1 \text{ Log } \eta^*}{\tilde{\delta}}\right).$$

Using the closure equations (37)-(39) gives:

$$\lim_{\mathscr{R}_\delta \to +\infty} (\widetilde{\bar{u}(x,z)})(x) = Q(x)\,\tilde{u}(x) \qquad (54)$$

$$\lim_{\mathscr{R}_\delta \to +\infty}\left(\widetilde{\frac{\partial \bar{u}(x,z)}{\partial z}}\right)(x) = \left(\frac{1-u_p(x)}{\tilde{\delta}(x)}\right) Q(x) \qquad (55)$$

with $u_p(x)$ given by (44) and $\tilde{u}(x)$ such that:

$$\tilde{u}(x) = (1.22 + u_p(x))/2.22. \qquad (56)$$

C. Modeling of equilibrium values for high Reynolds numbers

First of all, it can be seen that from definition (25) of $\Phi(x)$, we infer:

$$\int_0^\delta \frac{1}{\rho}\tau_{tur,\,eq}(x,z)\frac{\partial \bar{u}}{\partial z}(x,z)\,dz \simeq \Phi_{eq}(x)\frac{Q(x)^3}{2}. \qquad (57)$$

The expression of $\tilde{\mathscr{E}}_{eq}(x)$ is determined from the above model. To obtain the model of $\tilde{K}_{eq}(x)$ and $\tilde{\tau}_{eq}(x)$, we take the model developed in [28] which consists of introducing two models of $\frac{1}{\rho}\tau_{tur,\,eq}(x,z)$.. The first is a model of eddy viscosity:

$$\frac{1}{\rho}\tau_{tur,\,eq}(x,z) = 0{,}09\frac{K_{eq}(x,z)^2}{\mathscr{E}_{eq}(x,z)}\frac{\partial}{\partial z}\bar{u}(x,z) \qquad (58)$$

and the second is a mixing length model constructed on scale $\tilde{\delta}(x)$:

$$\frac{1}{\rho}\tau_{tur,\,eq}(x,z) = (0.09\,\tilde{\delta}(x))^2\left(\frac{\partial \bar{u}(x,z)}{\partial z}\right)^2. \qquad (59)$$

Applying the 1D approximation (50) to (58) and (59) gives two expressions of $\tilde{\tau}_{eq}(x)$ which are computed using (55) for $\mathscr{R}_\delta$ high. As model of $\tilde{\tau}_{eq}(x)$ we use that constructed from (59), and the model of $\tilde{K}_{eq}(x)$ is obtained by eliminating $\tilde{\tau}_{eq}(x)$ between the two expressions of $\tilde{\tau}_{eq}(x)$. This yields:

$$\left.\begin{aligned}\tilde{\tau}_{eq}(x) &= \underline{\tau}_{eq}(x)\,Q(x)^2;\\ \underline{\tau}_{eq}(x) &= [0.09\,(1-u_p(x))]^2\end{aligned}\right\} \qquad (60)$$

$$K_{eq}(x) = \underline{K}_{eq}(x)\,Q(x)^2; \qquad (61)$$

$$\left.\begin{aligned}\underline{K}_{eq}(x) &= \left[0.09\,(1-u_p(x))\frac{\Phi_{eq}(x)}{2}\right]^{1/2}\\ \tilde{\mathscr{E}}_{eq}(x) &= \underline{\mathscr{E}}_{eq}(x)\,Q(x)^3; \qquad \underline{\mathscr{E}}_{eq}(x) = \frac{\Phi_{eq}(x)}{2\tilde{\delta}(x)}\end{aligned}\right\} \qquad (62)$$

where $\tilde{\delta}(x)$ is defined by (41), $u_p(x)$ is defined by (44) and $\Phi_{eq}(x)$ is defined by (42).

III,3,5. — Modeling of the integral turbulence term $\mathscr{T}$

The term $\mathscr{T}(x)$ defined by (26) could be expressed directly by adding two transport equations to equations (12)-(14), one for $\langle u'^2\rangle$ and the other for $\langle w'^2\rangle$. But in this case, it would be necessary to proceed to modeling to ensure closure. Under these conditions, we preferred to directly model $\mathscr{T}(x)$. We therefore write:

$$(\langle u'^2\rangle - \langle w'^2\rangle)_{(x,\,z)} = h(x,z)\,K(x,z). \qquad (63)$$

It should be noted that if the turbulence were isotropic, we would have $h \equiv 0$, and if it were orthotropic with, for instance, $\langle v'^2\rangle = (0.8)^2\langle u'^2\rangle$, $\langle w'^2\rangle = (0.5)^2\langle u'^2\rangle$, we would have $h \equiv 0.8$. Here, this is not the case. Substituting (63) in (26) and using (48) and (50) gives:

$$\mathscr{T}(x) \simeq \rho\,\tilde{h}(x)\,\tilde{\delta}(x)\,\tilde{K}(x)$$

as well as, with (51), (61) and (41):

$$\mathscr{T}(x) = \rho\,Q(x)^2\,\delta_1(x)\,\tilde{\tilde{H}}(x)\,k(x) \qquad (64)$$

$$\tilde{\tilde{H}}(x) = \tilde{h}(x)\,(1-\eta^*(x))\,\underline{K}_{eq}(x)\,\alpha(x)^{-1}. \qquad (65)$$

We developed the following model of $\tilde{h}(x)$:

$$\tilde{h}(x) = C_{tur}\,\eta^*(x), \qquad C_{tur} \simeq 5. \qquad (66)$$

It can be seen that the model used gives $\tilde{h}(x) = 0$ and therefore $\mathscr{T}(x) = 0$] in the reattached region.

However, $\mathscr{T}(x)$ is nonzero in the upstream separated region. The value of the numerical constant C_{tur} was numerically identified from the experimental base [3].

III,4. — TRANSPORT EQUATIONS FOR THE SEPARATED-REATTACHED CASE

These equations are established here for the incompressible steady case at a high Reynolds number:

(1) The equation for $\tilde{K}$ is obtained by integrating (13) in z from 0 to $\delta(x)$, using (50) and (54) as well as equations (48), (51), (57) and EQE (30). The wall boundary conditions are explicitly inserted and the contribution of external turbulence is neglected.

(2) For the equation in $\tilde{\tau}$, the second member of (12) is transformed using model (58) of $\tau_{tur,\,eq}$, then

the transformed equation is integrated in z from 0 to $\delta(x)$. We then proceed as for the equation in $\tilde{K}$.

(3) The equation in $\tilde{\mathscr{E}}$ is obtained like the equation in $\tilde{K}$, starting from (14).

When the computations are conducted as indicated, we obtain (*see* [1]) the three transport equations sought for $\tilde{K}$, $\tilde{\tau}$ and $\tilde{\mathscr{E}}$:

$$\frac{d}{dx}(\tilde{\delta}\tilde{u}\tilde{K}Q)=\frac{\tilde{\tau}}{\tilde{\tau}_{eq}}\Phi_{eq}\frac{Q^3}{2}-\tilde{\mathscr{E}}\tilde{\delta} \tag{67}$$

$$\frac{d}{dx}(\tilde{\delta}\tilde{u}\tilde{\tau}Q)=-1{,}5\frac{\tilde{\delta}\tilde{\mathscr{E}}}{\tilde{K}}\left[\tilde{\tau}-\tilde{\tau}_{eq}\frac{\tilde{\mathscr{E}}_{eq}}{\tilde{\mathscr{E}}}\left(\frac{\tilde{K}}{\tilde{K}_{eq}}\right)^2\right] \tag{68}$$

$$\frac{d}{dx}(\tilde{\delta}\tilde{u}\tilde{\mathscr{E}}Q)=-1{,}5\frac{\tilde{\delta}\tilde{\mathscr{E}}}{\tilde{K}}\left[1{,}2\tilde{\mathscr{E}}-0{,}85\frac{\tilde{\tau}}{\tilde{\tau}_{eq}}\Phi_{eq}\frac{Q^3}{2}\right] \tag{69}$$

with $\tilde{\delta}$ given by (41) and $\tilde{u}$ by (56).

Equation (69) does not have an equilibrium solution such as $\frac{d}{dx}(\tilde{\delta}\tilde{u}\tilde{\mathscr{E}}Q)=0$. We will therefore preserve, as is suggested in [32], a model with two equations in $\tilde{K}$ and $\tilde{\tau}$, equation (69) being replaced by a closure equation constructed on the second equation (11) which gives:

$$\frac{\tilde{\mathscr{E}}(x)}{\tilde{\mathscr{E}}_{eq}(x)}=\left(\frac{l_{eq}}{l}\right)(x)\left(\frac{\tilde{K}(x)}{\tilde{K}_{eq}(x)}\right)^{3/2}. \tag{70}$$

In [28, 32], the authors use equation (70) with $\frac{l_{eq}}{l}(x)=1$. In the case at hand of a separated-reattached boundary layer, the work we did on the flat plate led us to construct another model and write:

$$\frac{\tilde{\mathscr{E}}(x)}{\tilde{\mathscr{E}}_{eq}(x)}=\lambda(x)\left(\frac{\tilde{K}(x)}{\tilde{K}_{eq}(x)}\right)^{3/2} \tag{71}$$

where:

$$\lambda(x)=1-\eta^*(x). \tag{72}$$

Thus, in the region where the boundary layer is attached, $\lambda(x)=1$ since $\eta^*(x)=0$, but in the upstream separated region, we have $\lambda(x)<1$ since in this case $\eta^*(x)>0$. Eliminating $\tilde{\mathscr{E}}$ from equations (67) and (68) using (71) and using notations (51) and the equilibrium equation (62) gives a model with two equations in k and τ:

$$\frac{d}{dx}\{Q(x)^3\tilde{\delta}(x)\tilde{u}(x)\underline{K}_{eq}(x)k(x)\}$$

$$=\frac{1}{2}\Phi_{eq}(x)Q(x)^3(\tau(x)-\lambda(x)k(x)^{3/2}) \tag{73}$$

$$\frac{d}{dx}\{Q(x)^3\tilde{\delta}(x)\tilde{u}(x)\underline{\tau}_{eq}(x)\tau(x)\}$$

$$=-1{,}5\times\frac{1}{2}\Phi_{eq}(x)Q(x)^3\frac{\underline{\tau}_{eq}(x)}{\underline{K}_{eq}(x)}$$

$$\times k(x)^{1/2}(\lambda(x)\tau(x)-k(x)^{1/2}) \tag{74}$$

With $\tilde{\delta}$, $\tilde{u}$, $\underline{K}_{eq}$, $\underline{\tau}_{eq}$, Φ_{eq} and λ given by (41), (56), (61), (60), (43) and (72) respectively.

III,5. — MODELING OF THE REGION NEAR THE LEADING EDGE

When developing the model for the upper surface boundary layer with separation on the leading edge and reattachment on the airfoil, we were led to drop the boundary layer equations for the first percentages of the upper surface $[0, x_A]$ and to use a so-called "geometric" model for this region. In effect, analysis of the experimental results [3] shows that for x_A on the order of 0.05 x_F (the first 5 percent), the pressure $p(x, 0)$ is quasi-constant. In addition, the rotational nature of the flow in this region means that the potential inviscid fluid predictor cannot be legitimately extended to compute the pressure in this region $x\in[0, x_A]$. The model used for the region near the leading edge is based on the following hypotheses:

(H6) The choice of the curvilinear abscissa x_A for a given problem must be such that:

(*a*) For $x\in[x_A, x_F]$ we have $|w(x, 0)/u(x, 0)|\ll 1$ which implies:

$$u(x, 0)\simeq q(x, 0)=Q(x), \qquad x\in[x_A, x_F] \tag{75}$$

(*b*) For $x\in[0, x_A]$, the pressure on the airfoil is nearly constant.

For instance, in the case of the plate [3], these two hypotheses are verified for $x_A\simeq 0.05\ x_F$.

(H7) With abscissa x_A fixed, the pressure on the airfoil is modeled in region $x\in[0, x_A]$ by constant extension with slope continuity. Thus, we write:

$$p(x, 0)=p(x_A, 0), \qquad x\in[0, x_A[\tag{76}$$

$$\frac{dp}{dx}(x_A, 0)=0 \quad \text{at point } x=x_A. \tag{77}$$

(H8) In region $x\in[x_A, x_F]$, the inviscid fluid is assumed irrotational. Bernoulli's theorem gives for $x\in[x_A, x_F]$:

$$C_p(x)=\left(\frac{1}{2}\rho\|V_\infty\|^2\right)^{-1}(p(x, 0)-p_\infty)$$

$$=1-Q(x)^2\simeq 1-u(x, 0)^2 \tag{78}$$

since $\|V_\infty\|=1$ and for $x\in[x_A, x_F]$, we have (35). Conditions (77) and (76) applied to (78) therefore imply:

$$\left(\frac{du(x,0)}{dx}\right)_{x=x_A}=0 \tag{79}$$

$$C_p(x)=C_p(x_A), \qquad x\in[0, x_A[\tag{80}$$

$$u(x,0)=u(x_A,0), \qquad x\in[0, x_A[. \tag{81}$$

Under these conditions, (H6) and (H7) imply a constant extension of $u(x, 0)$ to the value $u(x_A, 0)$ for $x\in[0, x_A[$ for the inviscid fluid predictor.

(H9) The boundary layer equations are valid for $x\in[x_A, x_F]$. Therefore, for $x\in[x_A, x_F]$, $u(x, 0)$ is computed by solving the boundary layer equations in inverse mode.

(H10) For $x\in[x_A, x_F]$, equation (28) is written as follows, considering (75):

$$w(x,0)\simeq\frac{d}{dx}(u(x,0)\,\delta_1(x)), \qquad x\in[x_A, x_F]. \tag{82}$$

In the geometric region $x\in[0, x_A[$, hypothesis (H6) no longer applies, since $w(x, 0)$ obtained by the inviscid fluid predictor is no longer small compared with $u(x, 0)=u(x_A, 0)$. In this region, $Q(x)$ differs from $u(x, 0)$. We therefore opted to model the displacement thickness $\delta_1(x)$ geometrically for $x\in[0, x_A[$, by extension of (82). Since $w(0,0)=\delta_1(0)=0$, we obtain:

$$\delta_1(x)=u(x_A,0)^{-1}\int_0^x w(\tilde{x},0)\,d\tilde{x}, \qquad x\in[0, x_A]$$

It should be noted that it is unnecessary to know δ_1 in region $x\in[0, x_A[$, since the boundary layer equations are solved for $x\in[x_A, x_F]$. However, (83) supplies the boundary conditions $\delta_1(x_A)$ and $\frac{d\delta_1}{dx}(x_A)$..

III,6. — UPPER SURFACE BOUNDARY LAYER EQUATION SOLVING METHOD

The upper surface boundary layer equations with the model introduced in Section III,5 are solved in inverse mode. To simplify the expression, the following notations are introduced:

$$\left.\begin{aligned}\tilde{\alpha}(x)=\alpha(x)^{-1}=\delta(x)\,\delta_1(x)^{-1},\\ \alpha\in]0,1], \qquad \tilde{\alpha}\in[1, +\infty[\end{aligned}\right\} \tag{84}$$

$$\tilde{H}(x)=H(x)^{-1}=\theta(x)\,\delta_1(x)^{-1}. \tag{85}$$

III,6,1. — New form of the boundary layer equations

The EQEA equation (31) is written using (52) and (84), for $x\in[x_A, x_F]$:

$$\delta_1(\tilde{\alpha}-1)\frac{dQ}{dx}+Q\frac{d}{dx}\{\delta_1(\tilde{\alpha}-1)\}=Q\,\tau\,C_{E_{eq}} \tag{86}$$

Starting from (29), using (75), substituting the expression of $w(x, 0)$ given by (28) and the expression of $\mathcal{T}$ given by (64), and considering notation (85), the EQK equation is written as follows for $x\in[x_A, x_F]$:

$$\frac{d}{dx}\{Q^2\delta_1(\tilde{H}-\tilde{\tilde{H}}k)\}+Q\frac{dQ}{dx}\delta_1=\frac{Q^2}{2}C_F \tag{87}$$

By differentiating the first member of (73) and (74) and dividing each member by Q^3, the transport equations in k and τ are written as follows for $x\in[x_A, x_F]$:

$$\frac{d}{dx}(Gk)=\frac{1}{2}\Phi_{eq}(\tau-\lambda k^{3/2})-3\left(\frac{1}{Q}\frac{dQ}{dx}\right)Gk \tag{88}$$

$$\frac{d}{dx}(F\tau)=-1{,}5\times\frac{1}{2}\Phi_{eq}\frac{\tau_{eq}}{\underline{K}_{eq}}(\lambda\tau k^{1/2}-k) -3\left(\frac{1}{Q}\frac{dQ}{dx}\right)F\tau \tag{89}$$

where we set:

$$G(x)=\tilde{\delta}(x)\,\tilde{u}(x)\,\underline{K}_{eq}(x) =(1-\eta^*(x))\tilde{u}(x)\,\underline{K}_{eq}(x)\,\tilde{\alpha}(x)\,\delta_1(x) \tag{90}$$

$$F(x)=\tilde{\delta}(x)\,\tilde{u}(x)\,\underline{\tau}_{eq}(x) =(1-\eta^*(x))\,\tilde{u}(x)\,\underline{\tau}_{eq}(x)\,\tilde{\alpha}(x)\,\delta_1(x). \tag{91}$$

III,6,2. — Equations and boundary conditions for computation of $\tilde{\alpha}$, k and τ

In inverse mode, for δ_1 and $\mathcal{R}_{\delta_1}$ given, functions $\tilde{\alpha}$, k and τ must be computed for $x\in[x_A, x_F]$ using three equations independent of Q. These equations are obtained by computing $\frac{1}{Q}\frac{dQ}{dx}$ from equation (86) and substituting this expression in (87)-(89). We thus obtain for $x\in[x_A, x_F]$:

$$\frac{1}{[1+2(\tilde{H}-\tilde{\tilde{H}}k)]}\frac{d}{dx}\{\delta_1(\tilde{H}-\tilde{\tilde{H}}k)\} -\frac{1}{\tilde{\alpha}-1}\frac{d}{dx}\{\delta_1(\tilde{\alpha}-1)\} =\frac{C_F}{2[1+2(\tilde{H}-\tilde{\tilde{H}}k)]}-\frac{\tau\,C_{E_{eq}}}{\tilde{\alpha}-1} \tag{92}$$

$$\frac{d}{dx}(G\,k)=\frac{1}{2}\Phi_{eq}(\tau-\lambda k^{3/2})$$
$$-\frac{3\,GC_{E_{eq}}}{\delta_1(\tilde{\alpha}-1)}k\tau$$
$$+\left[\frac{3\,G}{\delta_1(\tilde{\alpha}-1)}\frac{d}{dx}\{\delta_1(\tilde{\alpha}-1)\}\right]k \quad (93)$$

$$\frac{d}{dx}(F\tau)=-1{,}5\times\frac{1}{2}\Phi_{eq}\frac{\tau_{eq}}{\underline{K}_{eq}}(\lambda\tau k^{1/2}-k)$$
$$-\frac{3\,FC_{E_{eq}}}{\delta_1(\tilde{\alpha}-1)}\tau^2$$
$$+\left[\frac{3\,F}{\delta_1(\tilde{\alpha}-1)}\frac{d}{dx}\{\delta_1(\tilde{\alpha}-1)\}\right]\tau. \quad (94)$$

Since $u(x, 0)$ will be computed for $x\in[x_A, x_F]$ by the boundary layer equations and since condition (79) must be verified, a zero gradient must be imposed on parameter $\tilde{\alpha}$ at point x_A:

$$\frac{d\tilde{\alpha}(x)}{dx}=0, \qquad x=x_A. \quad (95)$$

Let $g_1\in\{\eta^*, C_3, u_p, \tau_{eq}, \tilde{u}, \lambda, \tilde{h}\}$, and $g_2\in\{C_1, C_2, C_F, H, \tilde{H}, C_{E_{eq}}, \Phi_{eq}, \underline{K}_{eq}, \tilde{H}\}$.

Algebraic closure shows that g_1 is a function of $\tilde{\alpha}=\frac{1}{\alpha}$ and g_2 is a function of $\tilde{\alpha}$ and Log $\mathscr{R}_{\delta_1}$. To construct the boundary conditions on point x_A, we introduce the following assumption:

$$\frac{d}{dx}\log\mathscr{R}_{\delta_1}\simeq 0, \qquad \text{in } x=x_A. \quad (96)$$

In this case, condition (95) implies:

$$\left(\frac{dg_1}{dx}\right)_{x=x_A}=0, \qquad \left(\frac{dg_2}{dx}\right)_{x=x_A}\simeq 0. \quad (97)$$

Equations (75), (79), (81)-(83), (95) and (97) allow us to write the following equations, determined from (86)-(88), at point $x=x_A$:

$$(\tilde{\alpha}-1)\frac{d\delta_1}{dx}\simeq\tau\,C_{E_{eq}} \quad (98)$$

$$\tilde{H}\frac{d\delta_1}{dx}-\tilde{\tilde{H}}\frac{d}{dx}(k\,\delta_1)\simeq\frac{C_F}{2} \quad (99)$$

$$[\tilde{\alpha}(1-\eta^*)\tilde{u}\,\underline{K}_{eq}]\frac{d}{dx}(k\,\delta_1)\simeq\frac{1}{2}\Phi_{eq}(\tau-\lambda k^{3/2}). \quad (100)$$

Eliminating $\frac{d}{dx}(k\,\delta_1)$ between (99) and (100) and substituting for τ its expression computed from (98) gives:

$$\tau(x_A)=\frac{1}{C_{E_{eq}}(x_A)}\left[(\tilde{\alpha}(x_A)-1)\frac{d\delta_1(x_A)}{dx}\right] \quad (101)$$

$$k(x_A)=\frac{1}{\lambda^{2/3}(x_A)}\left[\tau(x_A)-\frac{2\,\tilde{u}(x_A)}{\tilde{h}(x_A)\,\Phi_{eq}(x_A)}\right.$$
$$\left.\times\left(\tilde{H}(x_A)\frac{d\delta_1(x_A)}{dx}-\frac{C_F(x_A)}{2}\right)\right]^{2/3}. \quad (102)$$

In inverse mode, considering the closure algebra, it can be seen that the only independent boundary condition which must be supplied to the model is the value $\tilde{\alpha}(x_A)$ of $\tilde{\alpha}$ at point x_A, or, which amounts to the same thing, the value of the form parameter $H(x_A)$. As there is a strong separation at this point, an asymptotic value is introduced. In the case of the plate and PFSU, we verified that the solution obtained was relatively independent of this asymptotic value.

III,6,3. — *Equation for computation of* $u(x, 0)$

For δ_1 and $\mathscr{R}_{\delta_1}$ given, the solution of (92)-(94) with boundary conditions (101), (102), and $\tilde{\alpha}(x_A)$ given, allows $\tilde{\alpha}$, τ and k to be determined for $x\in[x_A, x_F]$. As these three functions are known, what must be done is to compute the velocity $u(x, 0)$ which will be used as given in the inviscid fluid predictor for strong coupling. Considering (75), $u(x, 0)$ must verify equation (86) which is written for $x\in[x_A, x_F]$:

$$\delta_1(x)\frac{du(x,0)}{dx}=\frac{1}{\tilde{\alpha}(x)-1}[\tau(x)\,C_{E_{eq}}(x)$$
$$-\frac{d}{dx}\{\delta_1(x)(\tilde{\alpha}(x)-1)\}]\,u(x, 0).$$

As this equation is homogeneous, a solution $\underline{u}(x)$ is constructed for $x\in[x_A, x_F]$ with the normalization condition (which may be arbitrary) $\underline{u}(x_F)=1$. Then model (81) is used for region $x\in[0, x_A]$. Under these conditions, $\underline{u}(x)$, $x\in[x_A, x_F]$ is the solution of:

$$\delta_1\frac{d}{dx}\underline{u}=\frac{1}{\tilde{\alpha}-1}\left[\tau\,C_{E_{eq}}-\frac{d}{dx}\{\delta_1(\tilde{\alpha}-1)\}\right]\underline{u} \quad (103)$$

$$\underline{u}(x_F)=1$$

and

$$\underline{u}(x)=\underline{u}(x_A) \qquad \text{for} \quad x\in[0, x_A] \quad (104)$$

then $u(x, 0)$ is written:

$$u(x, 0)=\gamma_Q\,\underline{u}(x) \qquad \text{for} \quad x\in[0, x_F]. \quad (105)$$

Constant γ_Q is determined when solving the strong

coupling by a trailing edge boundary condition (*see* Section IV).

IV. —STRONG COUPLING BETWEEN BOUNDARY LAYER AND INVISCID FLUID

IV,1. — NOTATIONS AND BOUNDARY CONDITIONS

To establish the strong coupling equations, a distinction is made between the upper surface variables (exponent +) and the lower surface variables (exponent −) and we set:

$$u^+(x)=u(x,0), \qquad w^+(x)=w(x,0), \qquad x\in(0,x_F),$$
$$u^-(x)=-u(x,0), \quad w^-(x)=-w(w,0), \quad x\in(x_F,x_T)$$

Considering (H4) and (H10), we have:

$$w^-(x)=0, \qquad x\in[x_F,x_T] \tag{107}$$
$$w^+(0)=\delta_1(0)=0,$$
$$w^+(x)=\frac{d}{dx}(u^+(x)\,\delta_1(x)), \qquad x\in[0,x_F]$$

On the trailing edge (point F), we must write $C_p^+(x_F)-C_p^-(x_F)=0$. In the case where the lower surface and upper surface normals are different at point F, the formulation we used (*see* below) to construct the inviscid fluid predictor leads to taking a pseudonormal on point F defined as the normal to the bisector of the angle formed by the lower surface and upper surface normals. The trailing edge boundary condition is then equivalent to:

$$w^+(x_F)=w^-(x_F) \tag{109}$$
$$u^+(x_F)=u^-(x_F). \tag{110}$$

Actually, we will not use (109) which will be a computation result.

IV,2. — CONSTRUCTION OF THE INVISCID FLUID PREDICTOR

As the upper surface boundary layer conditions are solved in inverse mode and since $w^-=0$ is known, the predictor must compute values $\{u^-, w^+\}$ for $\{u^+, w^-\}$ given.

Construction of the predictor is based on the hypotheses of an incompressible, steady, irrotational flow. It is written (*see* [1]):

$$\left[\begin{array}{c|c} N^{-+} & \pi+\Omega^{--} \\ \hline \pi+\Omega^{++} & -N^{+-} \end{array}\right]\left[\begin{array}{c} w^+ \\ \hline u^- \end{array}\right] = \left[\begin{array}{c|c} \Omega^{-+} & N^{--} \\ \hline -N^{++} & \Omega^{+-} \end{array}\right]\left[\begin{array}{c} u^+ \\ \hline w^- \end{array}\right] + \left[\begin{array}{c} F_\infty^- \\ \hline F_\infty^+ \end{array}\right] \tag{111}$$

where:

$$F_\infty^+(x)=2\pi(\beta_2(x)\sin\alpha_I+\beta_1(x)\cos\alpha_I, \qquad x\in OF_+$$
$$F_\infty^-(x)=-2\pi(\beta_2(x)\cos\alpha_I-\beta_1(x)\sin\alpha_I), \qquad x\in FO_-$$

where $\beta_1(x)$ and $\beta_2(x)$ are the components of the external normal in OXZ, $N^{s\sigma}$ and $\Omega^{s\sigma}$ are the kernel and solid angle operators such that:

$$f\mapsto(N^{s\sigma}f)(x) = \int_{x'\in C_\sigma} f(x')\frac{d}{dx}\operatorname{Log}R(x,x')\,dx', \qquad x\in C_s \tag{113}$$

$$f\mapsto(\Omega^{s\sigma}f)(x) = \int_{x'\in C_\sigma} f(x')\frac{d}{dx}\Theta(x,x')\,dx', \qquad x\in C_s \tag{114}$$

where $s\in\{+,-\}$, $\sigma\in\{+,-\}$.
$C_+=\widehat{OF}_+=\{x\,|\,x\in[0,x_F]\}$,
$C_-=\widehat{FO}_-=\{x\,|\,x\in[x_F,x_T]\}$, and where the integrals are taken in the sense of Cauchy for $s=\sigma$ and in the ordinary sense for $s\neq\sigma$.

Functions Θ and R are such that:

$$R(x,x')=((X(x')-X(x))^2+(Z(x')-Z(x))^2)^{1/2}$$
$$\Theta(x,x')=\operatorname{Arctan}\left[\frac{Z(x')-Z(x)}{X(x')-X(x)}\right]$$

where $(X(x), Z(x))$ are the cartesian coordinates in OXZ of a point of the airfoil with abscissa x.

IV,3. — STRONG COUPLING SOLVING METHODS

The problem is globally nonlinear and is solved by the fixed point method.

The predictor operator does not cause contraction. This is easily verified in the case in which the profile is an infinitely thin flat plate, when the eigenvalues of this operator have a modulus of 1. To make the fixed point convergent, we therefore introduced a relaxation on the predictor.

(1) The upper surface boundary layer is solved in inverse mode with the model developed in Section III.

The value of parameter $H(x_A)$ at point x_A is fixed. At the nth iteration of the fixed point, $\delta_1^{(n)}$, $\mathscr{R}_{\delta_1}^{(n)}$, $k^{(n)}$ and $\tau^{(n)}$ are known on the upper surface for $x \in [x_A, x_F]$. Equations (92)-(94), with boundary conditions (101), (102) are used to compute $\tilde{\alpha}^{(n+1)}$, $k^{(n+1)}$ and $\tau^{(n+1)}$ for $x \in [x_A, x_F]$. Knowing $\tilde{\alpha}^{(n+1)}$, $\tau^{(n+1)}$ for $x \in [x_A, x_F]$, equations (103) and (104) are used to compute $\underset{\sim}{u}^{+(n+1)}$ for $x \in [0, x_F]$. Under these conditions, the model can be used to make transformation CL^+.

$$\{\delta_1^{(n)}, \mathscr{R}_{\delta_1}^{(n)}, k^{(n)}, \tau^{(n)}\} \xrightarrow{CL^+} \{\underset{\sim}{u}^{+(n+1)}, \tilde{\alpha}^{(n+1)}, k^{(n+1)}, \tau^{(n+1)}\}. \quad (115)$$

(2) A relaxation with coefficient $1/\delta t$ is introduced in the predictor (111). The function $u^{+(n+1)}$ is given by (105): $u^{+(n+1)} = \gamma_Q \underset{\sim}{u}^{+(n+1)}$, constant γ_Q being computed by the boundary condition (110). Developing the boundary condition (107) and introducing:

$$\begin{pmatrix} \underset{\sim}{F}^{+(n+1)} \\ F^{-(n+1)} \end{pmatrix} = \begin{pmatrix} \Omega^{-+} \underset{\sim}{u}^{+(n+1)} \\ -N^{++} \underset{\sim}{u}^{+(n+1)} \end{pmatrix};$$

$$\begin{pmatrix} F^{+(n+1)} \\ F^{-(n+1)} \end{pmatrix} = \begin{pmatrix} \dfrac{\pi}{\delta t} u^{-(n)} + F_\infty^- \\ \dfrac{\pi}{\delta t} w^{+(n)} + F_\infty^+ \end{pmatrix}$$

$$\mathscr{A} = \left[\begin{array}{c|c} N^{-+} & \pi\left(1+\dfrac{1}{\delta t}\right)+\Omega^{--} \\ \hline \pi\left(1+\dfrac{1}{\delta t}\right)+\Omega^{++} & -N^{+-} \end{array}\right] \quad (117)$$

solution $\{w^{+(n+1)}, u^{-(n+1)}\}$ is then written (*see* [1]):

$$\begin{pmatrix} w^{+(n+1)} \\ u^{-(n+1)} \end{pmatrix} = \gamma_Q \begin{pmatrix} \underset{\sim}{G}^{+(n+1)} \\ \underset{\sim}{G}^{-(n+1)} \end{pmatrix} + \begin{pmatrix} G^{+(n+1)} \\ G^{-(n+1)} \end{pmatrix} \quad (118)$$

$$u^{+(n+1)} = \gamma_Q \underset{\sim}{u}^{+(n+1)}, \qquad w^{-(n+1)} = w^{-(n)} = 0 \quad (119)$$

where:

$$\begin{pmatrix} \underset{\sim}{G}^{+(n+1)} \\ \underset{\sim}{G}^{-(n+1)} \end{pmatrix} = \mathscr{A}^{-1} \begin{pmatrix} \underset{\sim}{F}^{+(n+1)} \\ \underset{\sim}{F}^{-(n+1)} \end{pmatrix};$$

$$\begin{pmatrix} G^{+(n+1)} \\ G^{-(n+1)} \end{pmatrix} = \mathscr{A}^{-1} \begin{pmatrix} F^{+(n+1)} \\ F^{-(n+1)} \end{pmatrix}$$

$$\gamma_Q = -\frac{G^{-(n+1)}(x_F^-)}{\underset{\sim}{G}^{-(n+1)}(x_F^-) - \underset{\sim}{u}^{+(n+1)}(x_F^+)}. \quad (121)$$

since $\mathscr{A}$ is independent of (n), we constructed its inverse outside the iterations. The predictor thus allows transformation $FP_{\delta t}$ to be made:

$$\{u^{-(n)}, w^{+(n)}, \underset{\sim}{u}^{+(n+1)}\} \xrightarrow{FP_{\delta t}} \{u^{-(n+1)}, w^{+(n+1)}, u^{+(n+1)}\}. \quad (122)$$

(3) Knowing $u^{+(n+1)}$ and $w^{+(n+1)}$ for $x \in [0, x_F]$, solving (108) allows $\delta_1^{(n+1)}$ to be computed for $x \in [0, x_F]$, then $\mathscr{R}_{\delta_1}^{(n+1)} = \mathscr{R} u^{+(n+1)} \delta_1^{(n+1)}$ for $x \in [x_A, x_F]$, i. e. to construct transformation ED^+:

$$\{w^{+(n+1)}, u^{+(n+1)}\} \xrightarrow{ED^+} \{\delta_1^{(n+1)}, \mathscr{R}_{\delta_1}^{(n+1)}\} \quad (123)$$

(4) In this algorithm for the fixed point, state $(n+1)$ is determined from state (n) by successively applying CL^+, $FP_{\delta t}$ and ED^+. The initialization is made on $u^{-(0)}$, $w^{+(0)}$, $\delta_1^{(0)}$. $\mathscr{R}_{\delta_1}^{(0)}$, $k^{(0)}$, $\tau^{(0)}$. We still have $w^- = 0$ and $H(x_A)$ fixed. For the convergence test, *see* Sec. V.

V. — NUMERICAL ANALYSIS

V,1. — MESH OF THE AIRFOIL

The upper surface (or lower surface) is meshed with M mesh cells of equal length, with step $\Delta x^+ = x_F/M$ (or $\Delta x^- = (x_T - x_F)/M$). Mesh cell j, $j \in \{1, 2, \ldots, 2M\}$ has as origin node the point noted m_j and as end node m_{j+1}, the center of the mesh being the point noted P_j and the unit normal external to point P_j being noted $\mathbf{n}_j$. The numbering increases with the curvilinear abscissa $x \in [0, x_T]$ such that m_1 is in O, m_{M+1} is in F and m_{2M+1} is in O.

V,2. — NUMERICAL APPROXIMATION OF $FP_{\delta t}$

The numerical approximation of mapping $FP_{\delta t}$ defined by (122) is obtained conventionally by approximating functions u^+, u^-, w^+, w^- by functions constant per mesh.

Matrices $[N^{s\sigma}] \in \mathrm{Mat}(M, M)$, $s, \sigma \in \{+, -\}$ correspond to breaking down matrix $[N] \in \mathrm{Mat}(2M, 2M)$ into blocks such that for any j and any j' in $\{1, \ldots, 2M\}$:

$$[N]_{jj'} = S_{jj'} \operatorname{Log}\left(\frac{\|\mathbf{P}_{j'}\mathbf{m}_{j+1}\|}{\|\mathbf{P}_{j'}\mathbf{m}_j\|}\right) \quad (124)$$

where $S_{jj'} = 1$ for j and j' in $\{1, \ldots, M\}$ or j and j' in $\{M+1, \ldots, 2M\}$; $S_{jj'} = \Delta x^-/\Delta x^+$ for $j \in \{1, \ldots, M\}$ and $j' \in \{M+1, \ldots, 2M\}$; $S_{jj'} = \Delta x^+/\Delta x^-$ for $j \in \{M+1, \ldots, 2M\}$ and $j' \in \{1, \ldots, M\}$.

Similarly, matrices

$$[\Omega^{s\sigma}] \in \mathrm{Mat}(M, M), \qquad s, \sigma \in \{+, -\}$$

correspond to breaking matrix $[\Omega] \in \mathrm{Mat}(2M, 2M)$ into blocks such that for any j and j' in $\{1, \ldots, 2M\}$,

$[\Omega]_{jj}=0$ and for $j \neq j'$:

$$[\Omega]_{jj'} = -S_{jj'} \left| \text{Arc cos} \left(\frac{\mathbf{P}_{j'}\mathbf{m}_j . \mathbf{P}_{j'}\mathbf{m}_{j+1}}{\| \mathbf{P}_{j'}\mathbf{m}_j \| \times \| \mathbf{P}_{j'}\mathbf{m}_{j+1} \|} \right) \right| \times \text{Sg} \{ (\mathbf{P}_{j'}\mathbf{m}_j + \mathbf{P}_{j'}\mathbf{m}_{j+1}) . \mathbf{n}_j \} \quad (125)$$

where Sg is the function "sign of".

V,3. — NUMERICAL APPROXIMATION OF CL^+

Let j_A be the index of node m_{j_A} with the value x_A introduced in III,5 as curvilinear abscissa.

We have $1 < j_A < M$. All the parameters involved are represented by their values at the nodes m_j of the upper surface mesh with curvilinear abscissa x_j, $j \in \{j_A, \ldots, M+1\}$.

The inverse solving mode leads to progressing from upstream to downstream. The derivatives with respect to x are therefore off-centered to the left.

(*a*) Let us set for $j \in \{j_A+1, \ldots, M+1\}$:

$$\text{FONC}_j(\tilde{\alpha}_j, k_j, \tau_j) = \frac{[D_j - (1/2) C_{F_j}]}{[1+2(\tilde{H}-\tilde{\tilde{H}}k)_j]} + \frac{|\tau_j C_{E_{eq}j} - D'_j]}{[\tilde{\alpha}_j - 1]}$$

$$D_j = (\Delta x^+)^{-1} [\{\delta_1 (\tilde{H}-\tilde{\tilde{H}}k)\}_j - \{\delta_1 (\tilde{H}-\tilde{\tilde{H}}k)\}_{j-1}]$$

$$D'_j = (\Delta x^+)^{-1} [\{\delta_1 (\tilde{\alpha}-1)\}_j - \{\delta_1 (\tilde{\alpha}-1)\}_{j-1}].$$

The numerical approximation of equation (92) is then written:

$$\text{FONC}_j(\tilde{\alpha}_j, k_j, \tau_j) = 0. \quad (126)$$

Equation (126) is used as follows. With the values k_{j-1}, τ_{j-1}, $(\delta_1)_{j-1}$, $\tilde{H}_{j-1}$, $\tilde{\tilde{H}}_{j-1}$, $\tilde{\alpha}_{j-1}$, $(\mathscr{R}_{\delta_1})_{j-1}$, k_j, τ_j and $(\mathscr{R}_{\delta_1})_j$ given, the solution in $\tilde{\alpha}_j$ is computed by a dichotomy method using the closure algebra.

(*b*) We set:

$$A_j = \frac{1}{2}\Delta x^+ \Phi_{eq\,j}; \qquad \tilde{A}_j = \frac{1}{2}\Delta x^+ \Phi_{eq\,j}\, 1{,}5 \left(\frac{\tau_{eq}}{K_{eq}} \right)_j$$

$$B_j = \Delta x^+ \left\{ \frac{3 G C_{E_{eq}}}{\delta_1(\tilde{\alpha}-1)} \right\}_j; \qquad \tilde{B}_j = \Delta x^+ \left\{ \frac{3 F C_{E_{eq}}}{\delta_1(\tilde{\alpha}-1)} \right\}_j$$

$$C_j = \left\{ \frac{3G}{\delta_1(\tilde{\alpha}-1)} \right\}_j [\{\delta_1(\tilde{\alpha}-1)\}_j - \{\delta_1(\tilde{\alpha}-1)\}_{j-1}];$$

$$\tilde{C}_j = \left\{ \frac{3F}{\delta_1(\tilde{\alpha}-1)} \right\}_j [\{\delta_1(\tilde{\alpha}-1)\}_j - \{\delta_1(\tilde{\alpha}-1)\}_{j-1}]$$

$$E_{j-1} = G_{j-1} k_{j-1}; \qquad \tilde{E}_{j-1} = F_{j-1} \tau_{j-1}$$

$$g_j^{(I)}(k, \tau) = G_j k - E_{j-1} - A_j(\tau - \lambda_j k^{3/2}) + B_j k \tau - C_j k;$$

$$g_j^{(II)}(k, \tau) = F_j \tau - \tilde{E}_{j-1} + \tilde{A}_j(\lambda_j \tau k^{1/2} - k) + \tilde{B}_j \tau^2 - \tilde{C}_j \tau.$$

The numerical approximation of (93) and (94) is then written as follows for $j \in \{j_A+1, \ldots, M+1\}$:

$$g_j^{(I)}(k_j, \tau_j) = 0, \qquad g_j^{(II)}(k_j, \tau_j) = 0. \quad (127)$$

These two equations are used as follows. With values A_j, B_j, C_j, E_{j-1}, $\tilde{A}_j$, $\tilde{B}_j$, $\tilde{C}_j$, $\tilde{E}_{j-1}$, λ_j, k_{j-1}, τ_{j-1} known, the solution (k_j, τ_j) of the nonlinear system (127) is computed by a Newton method.

(*c*) Finally, the numerical approximation of equation (103) is written for $j \in \{j_A, \ldots, M+1\}$:

$$\underline{u}_j^+ [(\delta_1)_j - \Delta x^+ \left\{ \frac{\tau C_{E_{eq}}}{\tilde{\alpha}-1} \right\}_j + \frac{1}{(\tilde{\alpha}_j - 1)} \Big(\{\delta_1(\tilde{\alpha}-1)\}_j - \{\delta_1(\tilde{\alpha}-1)\}_{j-1} \Big)] = (\delta_1)_j \underline{u}_{j-1}^+ \quad (128)$$

We take $\underline{u}_{j_A}^+ = 1$. $\underline{u}_{j_A+1}^+, \ldots, \underline{u}_{M+1}^+$, is then obtained directly by recurrence with (128) then this solution is normalized to have the condition introduced in (103): $\underline{u}_{M+1}^+ = 1$..

Finally, considering (104), $\underline{u}_j^+ = \underline{u}_{j_A}^+$, $j \in \{1, \ldots, j_A - 1\}$.

(*d*). We can then construct the numerical approximation of transformation CL^+ defined by (115).

Equation (126) in $\tilde{\alpha}$ is coupled with the two equations (127) in k and τ. The three nonlinear equations (126)-(127) are solved from upstream to downstream. They are used to construct mappings $\{\tilde{\alpha}_{j-1}, k_{j-1}, \tau_{j-1}\} \to \{\tilde{\alpha}_j, k_j, \tau_j\}$ for $j \in \{j_A+1, \ldots, M+1\}$ by recurrence, with the initial condition $(\tilde{\alpha}_{j_A}, k_{j_A}, \tau_{j_A})$. To compute the state at node j knowing the state at node $j-1$, (126)-(127) are solved by a local fixed point method. Convergence occurs rapidly and does not require relaxation, since the mapping causes contraction. Knowing $\tilde{\alpha}$, k and τ in all nodes $\{j_A, \ldots, M+1\}$, we compute $\underline{u}_j^+$, $j \in \{1, \ldots, M+1\}$ as indicated in point (*c*) above.

V,4. — NUMERICAL APPROXIMATION OF ED^+

The discretization of (108) with centered derivative directly gives the scheme from upstream to downstream. We have the following recurrence:

$$(u^+ \delta_1)_{j+1} = (u^+ \delta_1)_j + \Delta x^+ \underline{w}_j^+ \quad (129)$$

for $j \in \{1, \ldots, M\}$, where $(u^+ \delta_1)_1 = 0$ and where $\underline{w}_j^+ = w^+(P_j)$ is the value of the mesh cell center of w^+.

Recurrence (129) is solved in $(u^+ \delta_1)$. We then determine $(\delta_1)_j = (u^+ \delta_1)_j / u_j^+$.

V,5. — RELAXATION AND CONVERGENCE TESTS

(*a*) Let $f = (f_1, \ldots, f_{M+1}) \in \mathbf{R}^{M+1}$. We set:

$$\| f \|_M = \frac{1}{M+1} \left(\Sigma_{j=1}^{M+1} f_j^2 \right)^{1/2}. \quad (130)$$

The global fixed point convergence test we selected is an absolute test and is written:

$$\text{Sup}\{\|\delta_1^{(n+1)}-\delta_1^{(n)}\|_M, \|u^{+(n+1)}-u^{+(n)}\|_M, \|u^{-(n+1)}-u^{-(n)}\|_M\} \leqq \varepsilon_1. \quad (131)$$

(*b*) For each global iteration $(n+1)$, each node j and each local iteration (l) of the local fixed point defined in V,3-(*d*):

– the solution $\tilde{\alpha}_{j,l}^{(n+1)}$ of the nonlinear algebraic equation (126) constructed by dichotomy is computed with a relative tolerance constant ε_2;

– the solution $\{k_{j,l}^{(n+1)}, \tau_{j,l}^{(n+1)}\}$ of (127) constructed by the Newton method is computed with a relative tolerance constant ε_3.

(*c*) For each global iteration $(n+1)$ and each node j, the convergence test of the fixed local point (l) is:

$$|\tilde{\alpha}_{j,l+1}^{(n+1)}-\tilde{\alpha}_{j,l}^{(n+1)}) \leqq \varepsilon_l \tilde{\alpha}_{j,l+1}^{(n+1)}. \quad (132)$$

From this we infer that k_j and τ_j are determined in node j within ε_3 (in relative value).

(*d*) We calibrated constants ε_1, ε_2 and ε_3 in the framework of a parametric numerical analysis conducted on three airfoils: the flat plate [3] (*see* Section VI), the PFSU [43] and a bis-parabolic. All the processing was performed with $M=100$ (200 mesh cells on the upper surface and lower surface). We found $\varepsilon_1=10^{-6}$, $\varepsilon_2=10^{-6}$, $\varepsilon_3=10^{-7}$. The value ε_1 established corresponds to the smallest value which measures convergence outside the numerical background noise.

To decrease ε_1, it would be necessary to substantially increase M and decrease ε_2 and ε_3.

(*e*) The parametric numerical analysis mentioned in point (*d*) above also allowed us to calibrate the relaxation coefficient. We obtained $\frac{1}{\delta t}=5$, which value ensures rapid convergence of the global fixed point and is independent of the Reynolds number and the angle of attack for all the cases studied.

VI. — ANALYSIS OF THE FLAT PLATE AND COMPARISONS WITH EXPERIMENT

The flat plate considered is the one which was used for wind tunnel measurements [3].

Its geometry is defined by the diagram below with $L=0.200$, $e=0.006\,35$. The angle of attack $\alpha_I=4$ degrees and $\|\hat{\mathbb{V}}_\infty\| \simeq 30$ m/s.

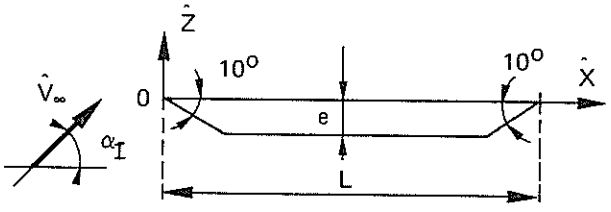

For the numerical model, we considered this plate to have zero thickness, i. e. a model equivalent to a cut. We used $M=100$ (200 mesh cells), $x_A=0.05$, $H(x_A)=30.9$, i. e. $\alpha(x_A)=0.741$, $\tilde{\alpha}(x_A)=1.35$ at $1/\delta t=5$.

VI,1. — RESULTS ON CONVERGENCE AND CPU TIMES

Let $E_n=-\log_{10}(\|f^{(n)}-f^{(n-1)}\|_M)$, where (n) is the number of the iteration of the global fixed point. Let N be the number of the last iteration such that the fixed point is converged. We note $\text{Max } f=\text{Sup}_{n\in\{1,\ldots,N\}} E_n$.

Figure 1 shows the convergence statistic for the three values $f\in\{\delta_1, u^-, u^+\}$.

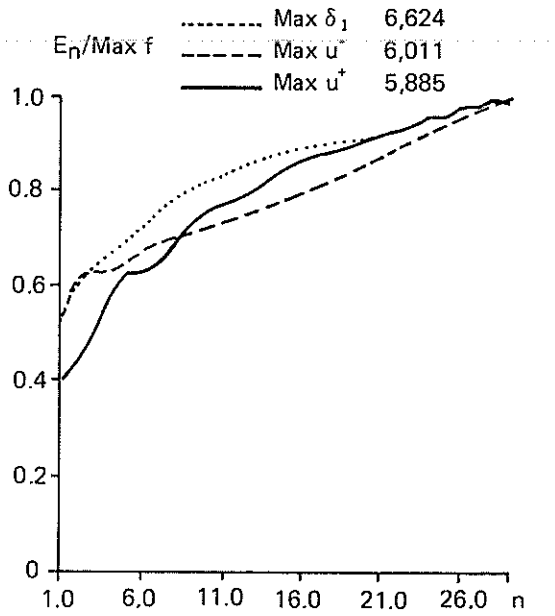

Fig. 1. – Statistic for $f\in\{\delta_1, u^-, u^+\}$. Abscissa: n=global fixed point iteration number. Ordinate: $E_n/\text{Max}\,f$ with $E_n=-\log_{10}(\|f^{(n)}-f^{(n-1)}\|)$. $\text{Max}\,f=\text{Sup}\,n\in\{1,\ldots,N\}\,E_n$. $N=29$: number of iterations to convergence.

n is read on the abscissa and in this case, $N=29$. $E_n/(\text{Max}\,f)$ is read on the ordinate and the values of $\text{Max}\,f$ are indicated. It can be seen that the convergence, obtained in 29 iterations, is relatively rapid.

For this computation configuration, the CPU time on the CYBER 855 is 4 seconds per iteration.

The CPU time spent for the initializations and preliminary computations is 24 seconds. The total CPU processing time is 140 seconds.

VI,2. — ANALYSIS OF THE RESULTS AND COMPARISONS WITH EXPERIMENT

The experimental results are those of publication [3]. Figure 2 is relative to C_p^+ and C_p^-. (positive and negative pressure coefficients).

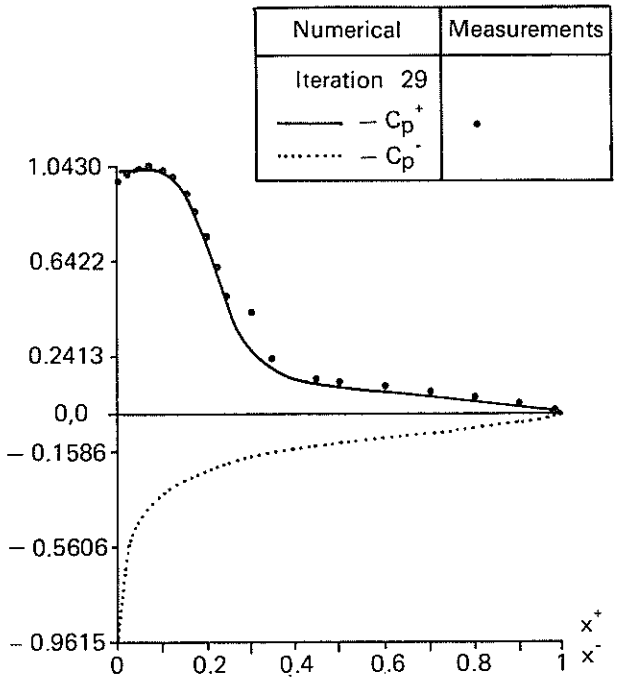

Fig. 2. – Comparison of numerical results and measurements for Cp^+ and Cp^-.

However, the C_p^- were not measured, which is why they are not shown. The good accuracy obtained for the model developed can be seen. The reattachment point found by the numerical method is at $x=0.31$ (31 percent). Figure 3 shows the comparisons between numerical predictions and measurements for the displacement thickness δ_1 and momentum thickness θ. Figure 4 is relative to the form parameter H. We did not show the experimental point H for

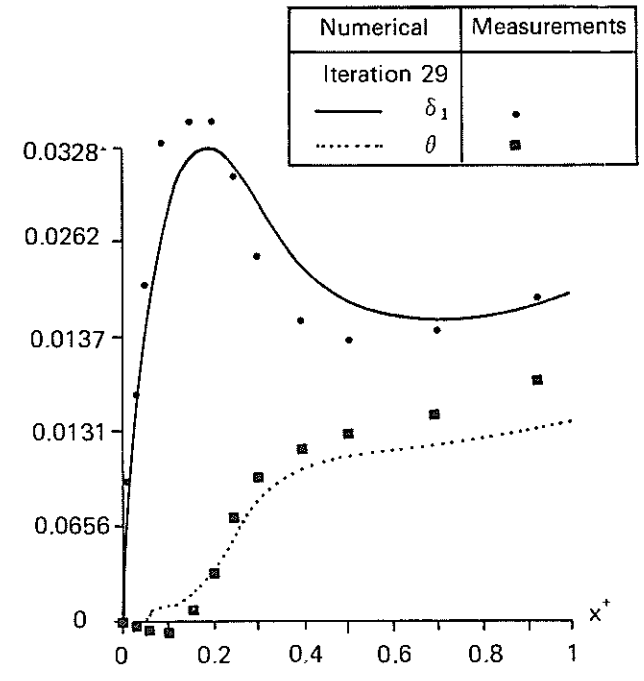

Fig. 3. — Comparison of the numerical results and measurements for δ_1 and θ.

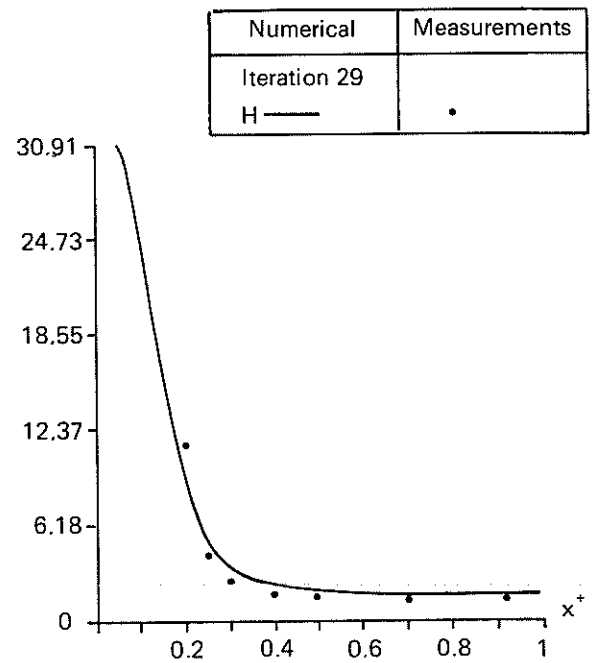

Fig. 4. — Comparison of the numerical results and measurements for H.

$x=0.15$ since, with a value of approximately 42, it is outside the graph.

Figure 5 shows the comparison for the turbulent integral friction. Figure 6 is relative to integral turbulence. Unfortunately, the direct comparison between the computations and measurements is not possible

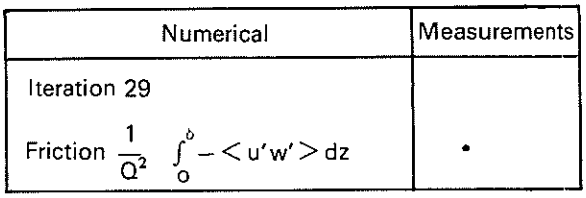

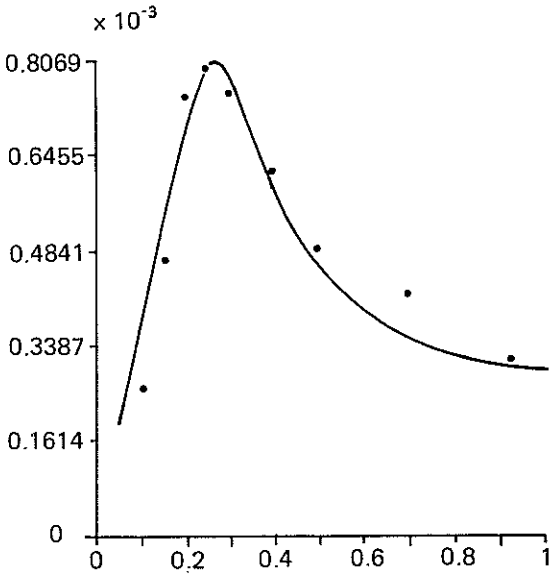

Fig. 5. — Comparison of the numerical results and measurements for integral turbulent friction.

Numerical	Measurements
Turbulence: $\frac{1}{Q^2}\int_0^\delta K\,dz$ $K=\frac{1}{2}\left(<u'^2>+<v'^2>+<w'^2>\right)$	▲ $\frac{1}{Q^2}\int_0^\delta K_{u'}\,dz$ • $2\times\frac{1}{Q^2}\int_0^\delta K_{u'}\,dz$ $K_{u'}=\frac{1}{2}<u'^2>$

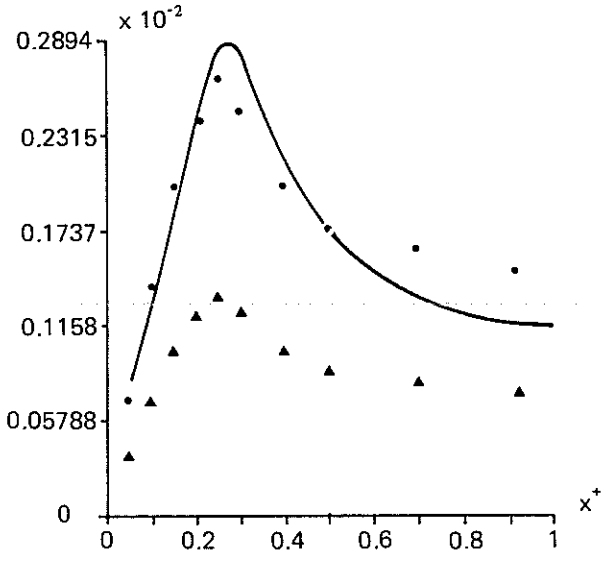

Fig. 6. — Integral turbulence. Numerical: total turbulence. Measurements: longitudinal turbulence.

for the following reasons. For the model, only the total turbulence, i. e. $T_{tot}(x)=Q(x)^{-2}\int_0^{\delta(x)} K(x,z)\,dz$, can be computed with $K=0.5\ (<u'^2>+<v'^2>+<w'^2>)$, whereas report [3] gives the integral turbulence relative to the longitudinal component, i. e. $T_{u'}(x)=Q(x)^{-2}\int_0^{\delta(x)} K_{u'}(x,z)\,dz$ with $K_{u'}=0{,}5<u'^2>$.

Figure 6 shows the measurements for $T_{u'}(x)$, which cannot be compared with the numerical results plotted for $T_{tot}(x)$. In addition, we plotted the measurements for $2\,T_{u'}(x)$. The factor 2 corresponds approximately to the factor we would have for a conventional orthotropic turbulence constant on the entire airfoil. This allows the levels to be displayed. We checked that the results on the whole depended very little on the values of x_A and $H(x_A)$. Table I illustrates this low dependency on two global values: (1) the lift normalized to the reference lift ($x_A=0.05$, $H(x_A)=30.9$, reference lift = 0.464 88) and (2) the abscissa of the reattachment point.

VII. — ANALYSIS OF THE PFSU AND COMPARISONS WITH EXPERIMENT

The PFSU is a Pflenminger-Sulzer blade profile used for steady and unsteady wind tunnel

TABLE I

Sensitivity of the results to parameters x_A and $H(x_A)$ for the plate.

x_A	$H(x_A)$	$\frac{\text{Lift}}{\text{Reference lift}}$	Abscissa of the reattachment point
0.02	30.8	0.995 2	0.30
0.03	30.8	0.994 6	0.30
0.04	30.9	0.996 5	0.30
0.05	30.9	1.000 0	0.31
0.05	23.2	0.993 4	0.31
0.05	25.1	0.995 2	0.31
0.05	28.4	0.998 0	0.31
0.05	30.9	1.000 0	0.31
0.05	33.8	1.001 9	0.31
0.05	39.0	1.004 8	0.31
0.05	43.2	1.006 8	0.31

measurements [43]. As was indicated, these measurements concern only the pressure coefficients (*see* Introduction).

The geometry of the PFSU normalized on the chord is defined by the diagram below. It is a symmetrical airfoil.

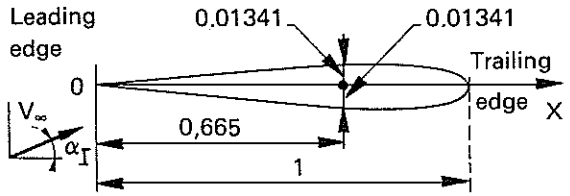

The analysis was made in the steady case for angles of attack of $\alpha_I=4$ degrees and $\alpha_I=5$ degrees, a Mach number of 0.300 and a Reynolds number $\mathcal{R}=2\,470\,000$. We used $M=100$ (200 mesh cells), $1./\delta t=5$. We did not attempt to adjust the value of $H(x_A)$. We took the raw values of the plate, i. e. $x_A=0.05$, $\tilde{\alpha}(x_A)=1{,}35$ which give, considering the Reynolds number, $H(x_A)=31.2$ for the two angles. The comparison of the pressure coefficients obtained with the measurements is given in Figures 7 and 8 for $\alpha_I=4$ degrees and $\alpha_I=5$ degrees, respectively, curves (2). On the same graphs, we also showed the results obtained by preserving $\tilde{\alpha}(x_A)=1.35$ but taking $x_A=0.02$. Here again, as for the plate, the value of this parameter is not very sensitive. It sets the length of the plateau [curves (1) on Figures 7 and 8].

Globally, the prediction is correct, but it is not as good as in the case of the plate (which was analyzed as a cut, i. e. infinitely thin) whereas for the PFSU, we introduced the exact profile. This divergence is relatively easy to explain in our opinion. It is due to the fact that on the last 10 percent of the PFSU, the lower surface boundary layer has a nonnegligible role and is not taken into account in the present model (*see* the conclusion below on this subject).

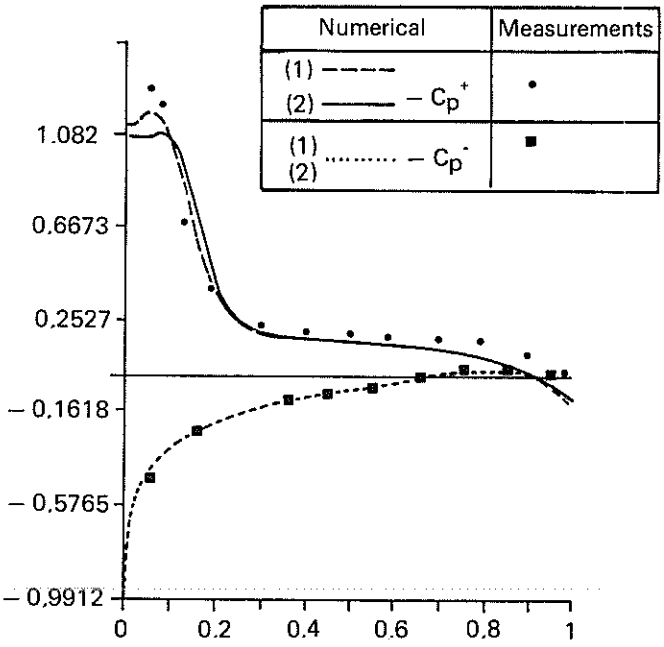

Fig. 7. — PFSU, angle of attack 4 degrees, Mach number 0.300, $\mathcal{R}=2\,470\,000$. (1) $x_A=0.02$, $H(x_A)=31.2$, $\tilde{\alpha}(x_A)=1{,}35$. (2) $x_A=0.05$, $H(x_A)=31.2$, $\tilde{\alpha}(x_A)=1.35$. Abscissa of reattachment point (1) and (2) = 0.22.

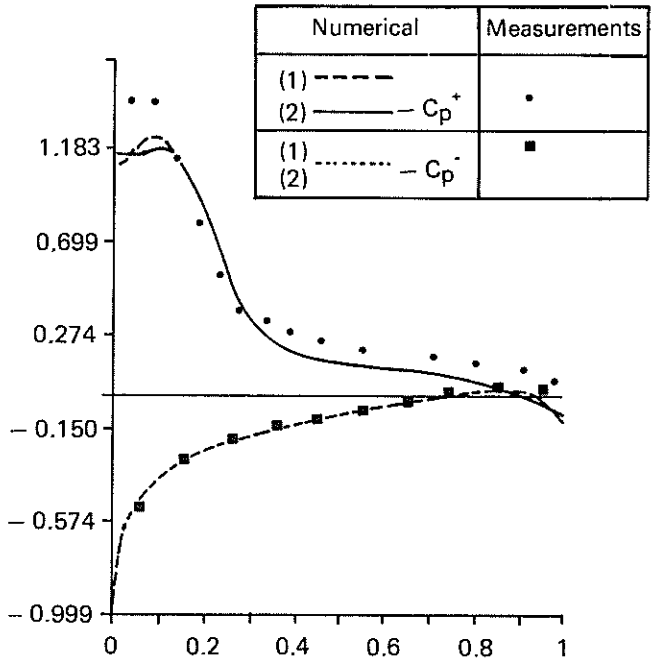

Fig. 8. — PFSU, angle of attack 5 degrees, Mach number 0.300, $\mathcal{R}=2\,470\,000$. (1) $x_A=0.02$, $H(x_A)=31.2$, $\tilde{\alpha}(x_A)=1{,}35$. (2) $x_A=0.05$, $H(x_A)=31.2$, $\tilde{\alpha}(x_A)=1.35$. Abcissa of reattachment point (1) and (2) = 0.33.

VIII. — CONCLUSION

The comparisons between the predictions supplied by the model developed and the measurements are satisfactory for the flat plate and the PFSU for the incompressible steady case. We effectively verified that the model was relatively insensitive to the value of parameters x_A and $H(x_A)$ introduced in the model. The small divergences obtained for the pressure coefficients of the PFSU are probably related to the fact that the lower surface boundary layer was not taken into account. Introduction of this boundary layer does not raise any problems, since it can be handled by conventional models and will be included in the second phase of development for the unsteady model which is the ultimate aim of this work.

This first phase allowed us to develop an upper surface boundary layer model for strong coupling between boundary layer and inviscid fluid in the case of leading edge separation with reattachment on the airfoil. Keeping in mind that the model will later be used for the unsteady case, we privileged computation efficiency and speed in developing it.

Manuscript submitted on April 23, 1987.

REFERENCES

[1] ANGELINI J. J. et SOIZE C. – *Étude théorique et numérique du couplage fort fluide parfait-couche limite dans le cas des grilles d'aubes. I. – Cas 2-D stationnaire incompressible :* Rapport 36/1621 RY 065 R. ONERA, (1987).

[2] ARNAL D., COUSTEIX J. et MICHEL R. – *Couche limite se développant avec gradient de pression positif dans un écoulement extérieur turbulent.* La Recherche Aérospatiale, 1976-1. English translation ESA-TT 351.

[3] BONNET J. L. et HOUDEVILLE R. – *Écoulement à l'extrados d'une place plane à bords aigus.* Rapport technique de synthèse 14/5014 DN, ONERA-CERT, (1986).

[4] BRADSHAW P. – *Prediction methods for turbulent flows. Calculation methods for complex flows.* VKI Lecture Series 76, (1975).

[5] BRADSHAW P., FERRIS D. H. and ATWELL N. P. – *Calculation of boundary layer development using the turbulent energy equation.* J. Fluid Mech., 28, (1967).

[6] BRADSHAW P. and PONTIKOS N. S. – *Measurements in the turbulent boundary layer or an infinite swept wing.* J. Fluid Mech., vol. 159, (1985).

[7] CEBECI T., CHEN L. T., CHANG K. C. and PEAVEY C. C. – *An iterative scheme for three-dimensional transonic flows.* Proceeding Third Symposium on Numeric and Physical Aspects of Aerodynamic Flows, California State University, USA, (1985).

[8] COLES D. – *The law of the wake in the turbulent boundary layer.* J. Fluid Mech., vol. 1. (1956) p. 191-226.

[9] COUSTEIX J. – *Progrès dans les méthodes de calcul des couches limites turbulentes bi et tri dimensionnelles.* 13e colloque d'aérodynamique appliquée, Lyon, France, (1976).

[10] COUSTEIX J. – *Couche limite avancée,* ENSAE, France, (1984).

[11] COUSTEIX J. – *Three dimensional and unsteady boundary layer computations.* Annual review of Fluid Mechanics, vol. 18, (1986) p. 173-196.

[12] COUSTEIX J., ARNAL D. et PAILHAS G. – *Étude expérimentale des couches limites avec turbulence extérieure*

et gradient de pression. N.T. 3/5014 DY, ONERA-CERT, (1975).

[13] COUSTEIX J., AUPOIX B. et PAILHAS G. – *Synthèse des résultats théoriques et expérimentaux sur les couches limites et sillages turbulents tridimensionnels,* N.T. 4, ONERA, (1980).

[14] COUSTEIX J. and QUEMARD C. – *Velocity profiles and shear stress of three dimensional turbulent boundary layers.* T.P. 1134, ONERA, (1972).

[15] COUSTEIX J., QUEMARD C. et MICHEL R. – *Application d'un schéma amélioré de longueur de mélange à l'étude des couches limites turbulentes tridimensionnelles,* AGARD CP, n° 93, On turbulent shear flows, (1971).

[16] CROSS A. G. T. – *Calculation of compressible three-dimensional turbulent boundary layers with particular reference to wings and bodies.* British Aerospace Brough YAD, (1979).

[17] EAST L. F. and SAWYER W. G. – *An investigation of the structure of equilibrium turbulent boundary layers* AGARD CP, n° 271, (1971).

[18] FAVRE A., KOVASZNAY L. S. G., DUMAS R., GAVIGLIO J. COANTIC M. – *La turbulence en mécanique des fluides,* Gauthier-Villars, (1976).

[19] GREEN J. E., WEEKS D. J. and BROOMAN J. W. F. – *Prediction of turbulent boundary layers and wakes in incompressible flow by a lag entrainment method.* RAE TR 72231, (1972).

[20] HINZE J. O. – *Turbulence. An introduction to its mechanism and theory.* Mc Graw-Hill, New York, (1959).

[21] KLINE S. J., CANTWELL B. J. and LILLEY G. M. – AFOSR-HTTM STANFORD Conference on complex turbulent flows, (1980-1981).

[22] KLINE S. J., MORKOVIN M. V., SOVRAN G. and COCKRELL D. J. – *Computation of turbulent boundary layers.* AFOSR-IFP STANFORD Conference, (1968).

[23] LAUNDER B. E. – *Production methods for turbulent flows progress in the modeling of turbulent transport.* VKI Lecture Series 76, (1975).

[24] LAUNDER B. E. and SPALDING D. B. – *Lectures in mathematical models of turbulence.* Academic Press, New York, (1975).

[25] LE BALLEUR J. C. – *Couplage visqueux-non visqueux : Analyse du problème incluant décollements et ondes de choc.* La Recherche Aérospatiale, n° 1977-6. English translation ESA-TT 476.

[26] LE BALLEUR J. C. – *Couplage visqueux-non visqueux : Méthode numérique et applications aux écoulements tridimensionnels transsoniques et supersoniques.* La Recherche Aérospatiale, n° 1978-2. English translation ESA-TT 496.

[27] LE BALLEUR J. C. – *calcul des écoulements à forte interaction visqueuse au moyen des méthodes de couplage,* AGARD CP 291, General introduction, Colorado Springs, (1981), and ONERA TP 1980-121.

[28] LE BALLEUR J. C. — *Strong matching method for computing transonic viscous flows including wakes and separations. Lifting airfoils.* La Recherche Aérospatiale, n° 1981-3. French and English editions.

[29] LE BALLEUR J. C. – *Viscid-inviscid coupling calculations for two and three dimensional flows.* VKI Lecture Series 1982-04, and Computational Fluid Dynamics, (1982).

[30] LE BALLEUR J. C. – *Numerical viscid-inviscid interaction in steady and unsteady flows.* Proceeding 2nd Symposium on numerical and physical aspects of aerodynamic flows, California State University, USA, and ONERA TP 1983-8.

[31] LE BALLEUR J. C. and BLAISE D. — *Computation of internal separated flows and shock wave-boundary layer interactions by viscous-inviscid interaction.* La Recherche Aérospatiale, n° 1985-4, French and English editions.

[32] LE BALLEUR J. C. and GIRODOUX-LAVIGNE P. — *A semi-implicit and unsteady numerical method of viscous-inviscid interaction for transonic separated flows.* La Recherche Aérospatiale, n° 1984, 1, French and English editions.

[33] LESLIE D. C. – *Developments in the theory of turbulence.* Clarendon Press, Oxford, (1973).

[34] LOISEAU H. and SZECHENY E. – *Aeroelasticity of compressor blades. Subsonic stall flutter.* La Recherche Aérospatiale, n° 1981-6, French and English éditions.

[35] LUMLEY J. L. – *Prediction methods for turbulent flows. Introduction.* VKI Lecture Series 76, (1975).

[36] MELNIK R. E., HEAD H. R. and JAMESON A. – *A multi-grid method for the computation of viscid-inviscid interaction on airfoils.* AIAA Paper 83-0234, Reno, (1983).

[37] MICHEL R. – *Couches limites, frottement et transfert de chaleur.* Cours de l'ENSAE.

[38] MICHEL R., QUEMARD C. et COUSTEIX J. – *Méthode pratique de prévision des couches limites turbulentes bi et tri dimensionnelles.* La Recherche Aérospatiale, n° 1972-1.

[39] MICHEL R., QUEMARD C. et DURANT R. – *Application d'un schéma de longueur de mélange à l'étude des couches limites d'équilibre.* ONERA N.T. 154, (1969).

[40] MORTCHELEWICZ G. D. – *Calcul des écoulements instationnaires en grilles d'aubes,* RT ONERA n° 29/162 RY080R, (1983).

[41] MORTCHELEWICZ G. D. and ANGELINI J. J. — *Computation of unsteady aerodynamic pressure coefficients in a transonic straight cascade.* La Recherche Aérospatiale, n° 1984-3, French and English editions.

[42] MYRING D. F. – *An integral prediction method for three-dimensional turbulent boundary mayers.* RAE-TR 70147, (1970).

[43] NOTIN C. – *Étude de l'écoulement autour d'un profil d'aube de compresseur en régime subsonique.* Rapport 34/1621 RY 046 R, ONERA, (1985).

[44] OKUNO T. – *Distribution of wall shear stress and cross flow in three-dimensional turbulent boundary layer* on ship hull. Journ. Soc. Nav. Arch., Japan, vol. 139, (1976).

[45] REYNOLDS W. C. – *Computation of turbulent flows.* Annual Review of Fluid Mechanics, vol. 8, (1979).

[46] ROTTA J. C. – *A family of turbulence models for three-dimensional boundary layers. Turbulent shear flow I.* Springer Verlag, Berlin, (1979).

[47] SAFFMAN P. G. and WILROX D. C. – *Turbulence model predictions for turbulent boundary layers,* AIAA Journal, vol. 12, n° 4, (1972).

[48] SCHLICHTING H. – *Boundary layer theory.* McGraw-Hill, New York, (1968).

[49] SCHMITT V. and COUSTEIX J. – *Boundary layers on a swept wing up to high angles of attack. Euromech* 60, Trondheim, (1975).

[50] SMITH P. D. – *An integral prediction method for three-dimensional compressible turbulent boundary layers,* ARC Rand M 3739, (1972).

[51] TENNEKES H. 1nd LUMLEY J. L. – *A first course in turbulence.* MIT Press, (1972).

[52] TOWNSENS A. A. – *The structure of turbulent shear flow.* Cambridge University Press, (1976).

[53] WHITFIELD D. L., SWAFFORD T. W. and JACOCKS J. L. – *Calculation of turbulent boundary layers with separation, reattachment and viscous-inviscid interaction.* AIAA Paper, 80-1439, (1980).